FREE-STREAMLINE ANALYSES OF TRANSITION FLOW AND JET DEFLECTION

Edited by

JOHN S. McNOWN

and

CHIA-SHUN YIH

State University of Iowa
Studies in Engineering
Bulletin 35

Published by the State University of Iowa

No. 427

FREE-STREAMLINE ANALYSES OF TRANSITION FLOW AND JET DEFLECTION

Edited by

JOHN S. McNOWN
Associate Director
and
CHIA-SHUN YIH
Research Engineer
Iowa Institute of Hydraulic Research

Publication supported by the
Graduate College
State University of Iowa
and the
Office of Naval Research

Published by the University
Iowa City, Iowa
1953

TABLE OF CONTENTS

Page

Elements of Free-Streamline Theory, John S. McNown ... 3

Transition Curves of Constant Pressure

I. Streamlined Struts, R. Gerber and John S. McNown 15

II. Inlets, D. W. Appel and E. M. Laursen ... 21

Deflection of Jets

I. Symmetrically Placed V-Shaped Obstacles, T. T. Siao and P. G. Hubbard ... 33

II. Symmetrically Placed ⊔-Shaped Obstacles, Turgut Sarpkaya ... 45

III. Unsymmetrically Placed Semi-Infinite Plate, Simon Ince and Clark DeHaven ... 54

Manifold Efflux, Arthur Toch and Robert W. Moorman ... 63

Head Losses in Miter Bends, Harry H. Ambrose ... 73

References ... 81

ELEMENTS OF FREE-STREAMLINE THEORY

by

JOHN S. McNOWN*

INTRODUCTORY REMARKS

Many plane irrotational flow patterns which include the formation or deflection of free jets can be analyzed completely by a method known as the Helmholtz-Kirchhoff theory of free streamlines. The results obtained may be significant not only for the corresponding two-dimensional flows of real incompressible fluids but, in some instances, for their three-dimensional counterparts as well. Numerous worthwhile calculations remain to be made, perhaps because the theoretician and the hydraulician have not yet pooled their interests for effective exploitation of this powerful tool. The analyses consist of the definition of successive conformal transformations involving a hodograph, or velocity plane, and the application of the Schwarz-Christoffel transformation. A number of such calculations are presented in the following articles.

Impetus for the preparation of this bulletin came from the writer's earlier contact with Professor W. E. Brooke (Chairman Emeritus of the Mathematics and Mechanics Department, University of Minnesota), and from suggestions by Professor Kravtchenko (Faculté d s Sciences, Université de Grenoble) and M. DuPort (Engineer at the Etablissements Neyrpic, also in Grenoble). The second paper was prepared by M. Gerber and the writer, at Kravtchenko's suggestion, in order to obtain a comparison of the results of theory with those from experiments with cavitating flows. The remaining papers were prepared subsequently by second- and third-year graduate students in the department of Mechanics and Hydraulics at the State University of Iowa. This cooperative endeavor was undertaken as an experiment in combining teaching with the conduct of original investigation. These selecte i students, many of whom are also staff members of the Iowa Institute of Hydraulic Research, began with a literature

*Associate Director, Iowa Institute of Hydraulic Research, State University of Iowa, Iowa City.

survey and a group review of the essential theory, and then completed the detailed analyses and calculations of the various problems selected. Formal oral reports were coordinated and presented to an audience composed of faculty members and other graduate students, and the pedagogical experiment was completed by the preparation of the remainder of the papers in this bulletin. Mr. Carstens of the Department of Engineering English provided valuable criticism and assistance in their preparation. Financial assistance was provided by the Office of Naval Research (N8onr-500 TO 3) for the conduct of the experiments and for the editing and publication of this Bulletin.

HISTORICAL DEVELOPMENT

During the period of over eighty years which has elapsed since the original developments of Helmholtz [1]* and Kirchhoff [2], the numerous contributions to this intriguing phase of analytic function theory have been made primarily by mathematicians, with results which sometimes appear bizarre from the practical point of view. Aside from a few classic cases which were solved before 1900 [1, 2, 3], the kinds of flows analyzed have usually been significant more

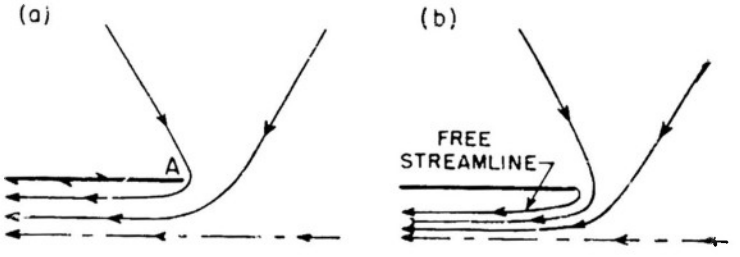

FIG. 1. COMPARISON OF ENTRANCE CONDITIONS
(a) NO SEPARATION; (b) FREE STREAMLINE

for the mathematical method than for the result. The mathematician has seldom been interested in the applications of the subject, whereas the hydraulician with much to gain has equally rarely acquainted himself with the theory sufficiently well even to make suggestions to the theoretician. Thus with only occasional exceptions, such as the works of von Mises [4] and, much more recently, Birkhoff et al [5] and Plesset and Shaffer [6], little of value to the prac-

*References for all of the papers are collected at the end of this Bulletin.

titioner has been presented in the numerous works on this subject since publication of the earliest papers.

Helmholtz devised the concept of the free streamline in a search for a more realistic solution to the problem of efflux from (or flow into) a two-dimensional pipe or channel. The only prior classical theory was for flow which doubled back on the boundary in such a way as to give infinite velocities and negatively infinite pressures at the end of the channel (point A in Fig. 1a). His fundamental contribution was the concept of a free boundary which was defined in the kinematic rather than in the geometric sense (Fig. 1b). He

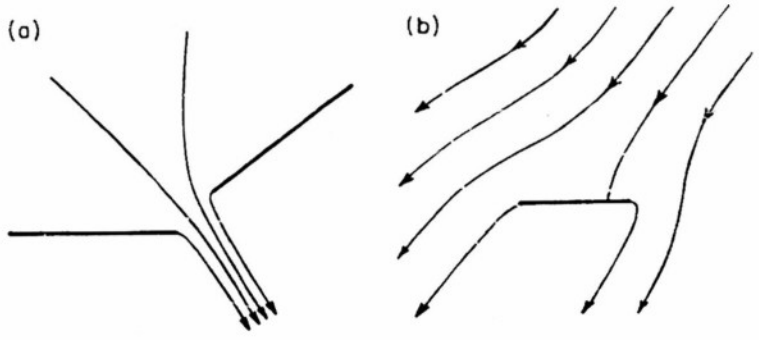

FIG. 2. FLOW PATTERNS FOR (a) SLOT, AND (b) FLAT PLATE

reasoned logically that the bounding streamline would separate from the solid boundary, and that the free streamline thus formed could be characterized by a constant pressure and, hence, by a constant velocity. He visualized a quiescent wake of constant pressure and a velocity discontinuity at the free streamline. With the aid of this concept, he proceeded to derive the equations for the free jet issuing from a Borda tube. Kirchhoff shortly afterwards devised functions for the description of the efflux from an opening in an infinite reservoir having plane boundaries, and of the effect of a plate on a field of flow which is otherwise uniform and extends to infinity in all directions (Fig. 2). Rayleigh [3] systematized these results somewhat and added his analysis of intersecting jets. The method employed by these pioneers was indirect in that it consisted of trying various functions and adjusting constants until some useful result was obtained.

Development of a direct method of solving any of a large class of free-streamline flows awaited definition of the hodograph planes and certain complementary transformations. The ordinary hodo-

graph or velocity plane was first used by Michell [7] in conjunction with the well known transformation

$$t = \frac{1}{2}\left(\zeta + \frac{1}{\zeta}\right)$$

Planck [8] in 1894 suggested the logarithmic hodograph which, together with the important transformation theorem developed by Christoffel [9] in 1867 and independently by Schwarz [10] in 1869, made possible the direct resolution of flow patterns for a wide variety of boundary configurations. The primary restrictions on the method, aside from complexity of detail, were the general considerations that the motions be two-dimensional, incompressible, and unaffected by gravity or viscosity, and that the solid boundaries be composed of rectilinear segments.

In the interval between 1890 and 1920 a number of contributions were made of flow patterns for a variety of boundary conditions. With the exception of the very few papers on the simplest and most fundamental problems and of the paper by von Mises [4], already mentioned, few calculated results were presented, the authors being content to give general results or simply to indicate their existence.

Not until the past few years has there been any renewal of interest in the extension and application of this type of analysis to obtain useful results in current investigations. Recently, Birkhoff, Plesset, and others have published studies of boundary effects in cavity flows, and Salzman [11] and McNown and Hsu [12] have published analyses of lateral efflux through an opening in one side of a two-dimensional channel. Comparisons of the results of theory and of experiment have indicated a correspondence which is usually close and sometimes astonishingly so.

THE HODOGRAPH PLANES

In the derivation of functional relationships which make possible the mathematical description of a pattern of flow, definition of a hodograph or velocity plane is an essential step. Two types are used which differ in detail but are similar in concept in that they make possible the comparatively simple representation of the complicated bounding streamlines. These two planes, on which the flow patterns are transformed conformally in accordance with the

precepts of complex-function theory, can best be described through presentation in connection with a specific example.

If $w = \phi + i\psi$ represents the complex potential and $z = x + iy$ the variable in the plane of actual flow, the equation

$$w = f(z)$$

indicates the relationship sought. A fundamental concept of hydrodynamics is that

$$\frac{dw}{dz} = -u + iv = -qe^{-i\theta}$$

in which u and v are the x- and y-components of the velocity at any point, q is the magnitude of the resultant velocity, and θ is its inclination measured from the x-axis, as shown in Fig. 3. Thus,

$$q = +\sqrt{u^2 + v^2} \quad , \quad \theta = \tan^{-1}\frac{v}{u}$$

If, to simplify the terminology, ζ is substituted for dw/dz, the two kinds of hodographs commonly used are representations of ζ and

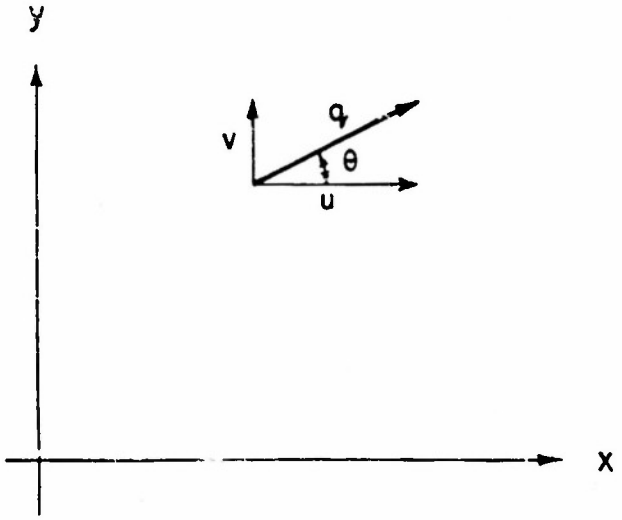

FIG. 3. DEFINITION SKETCH FOR VELOCITY.

of $\Omega = \ln(-V_j/\zeta)$, the second being also expressible in the form

$$\Omega = \ln\left(-V_j\frac{dz}{dw}\right) = -\ln\frac{q}{V_j} + i\theta$$

Straight solid boundaires in the z-plane transform into radial lines in the ζ-plane (u/v = constant), and into straight lines parallel to the real axis (θ = constant) in the Ω-plane. Furthermore,

free streamlines, along which the pressure and velocity are constant in the z-plane, become circular arcs with centers at the origin ($u^2 + v^2 =$ constant) in the ζ-plane, and straight lines parallel to the imaginary axis ($q =$ constant) in the Ω-plane. It is thus evident that the original boundary transforms into either a circular sector or a rectangle.

As an illustration of this method, the four planes, (z, ζ, Ω, and w) are shown in Fig. 4a for the unsymmetrical efflux from a two-dimensional channel, corresponding points having been assigned the same letter in each plane. For mathematical simplicity, a reference velocity such as V_j is often assigned the value unity. This has not been done herein so that the physical significance of the variables would not be altered. The points A and D represent regions far to the left and far to the right, respectively, at which the velocity is constant. The ϕ- and ψ-lines in the w-plane are vertical and horizontal as always, and, for this case of finite quan-

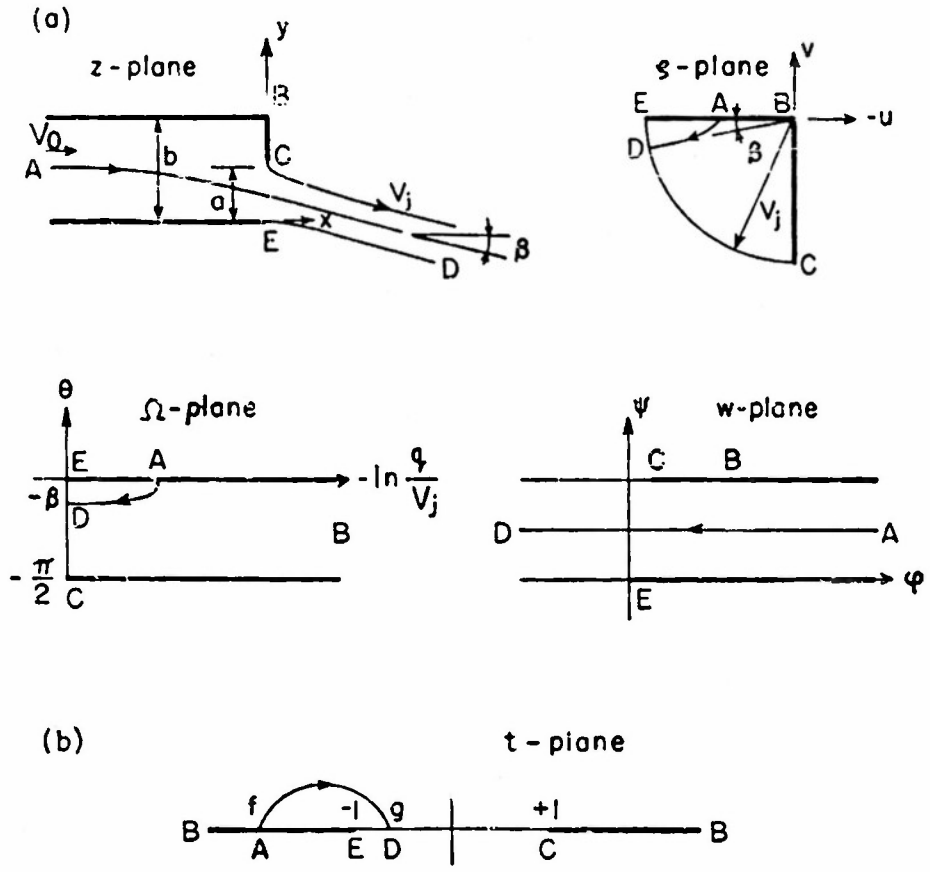

FIG. 4. CONFORMAL MAPPING PLANES.

tity of flow, the boundary of the flow in the w-plane becomes a rectangle of finite width $(0 \leqq \psi \leqq V_0 b)$ and infinite length $(-\infty \leqq \phi \leqq \infty)$. The coordinates of the various points are indicated in Table I; the t-plane is discussed in the following section.

TABLE I

	z	ζ	Ω	w	t
A	$-\infty + i(0 \text{ to } b)$	$-V_0$	$-\ln(V_0/V_j)$	$\infty + i(0 \text{ to } V_0 b)$	$f = -\frac{1}{2}\left(\frac{V_0^2}{V_j^2} + \frac{V_j^2}{V_0^2}\right)$
B	ib	0	$\infty + i(0 \text{ to } -\pi/2)$	$\phi_B + iV_0 b$	∞
C	ia	$-iV_j$	$-i(\pi/2)$	$\phi_C + iV_0 b$	1
D	undefined	$-V_j e^{i\beta}$	$-i\beta$	$-\infty + i(0 \text{ to } V_0 b)$	$g = -\cos 2\beta$
E	0	$-V_j$	0	0	-1

As the regions at A and D become points in the ζ- and Ω-planes, the concept of flow from a point source to a point sink within prescribed boundaries is useful for the interpretation of these intermediate planes. That is, they are not only plots of the velocity, but transformed flows as well; intermediate streamlines are indicated in the several planes. The necessary simplification of the boundary has been accomplished by the representation in either the ζ- or the Ω-plane. The links between the several planes remain to be defined.

DEFINITION OF TRANSFORMATIONS

In order to utilize the planes in the definition of the essential functional relationship between w and z, either ζ or Ω must be related to w by means of known methods through still another complex variable designated as t. This relationship completes the rather complicated functional analysis because, as has already been pointed out, either ζ or Ω can be expressed in terms of dw/dz. The only remaining difficulties arise in the explicit evaluation of the various functions which are initially known only as differential equations.

Any polygonal boundary in one complex plane can be transformed into the entire real axis of another through application of the Schwarz-Christoffel theorem, the interior of the polygon being

transformed into either the upper or the lower half of the second plane [13]. Thus the outline in the Ω-plane and that in the w-plane are directly transformable into the real axis of the t-plane as shown in Fig. 4b. The transforming function can be written as follows:

$$\Omega = M \int \frac{dt}{(t-t_1)^{\beta_1/\pi}\,(t-t_2)^{\beta_2/\pi}\,\ldots\,} + N$$

As many factors $(t-t_n)$ are introduced into the transformation as there are vertices of the polygonal boundary in the Ω-plane (see Fig. 5). The value t_n is the locus of the transformed point on the real axis in the t-plane, and β_n is the exterior angle of the polygon at that point in the Ω-plane. Three of the t_n-values can be assigned arbitrarily and the remainder must be given parametric values to be evaluated in terms of given quantities, along with M and N, from the integrated function. Points for which t_n is infinity need not be included no matter what the value of β_n. If the interior angle exceeds π, the exterior angle, as well as the corresponding exponent, becomes negative.

In defining the transformation between Ω and t for the example of Fig. 4, the points B, C, and E are arbitrarily placed in the t-plane at ∞, $+1$, and -1, respectively. The unknown or parametric values of the abscissas at A and D are assigned the values f and g. The vertices of the polygon are at the points B, C, and E for which the exterior angles are π, $\pi/2$, and $\pi/2$. Because B is placed at ∞, the only terms to be included are those at C and E, and the transformation becomes a familiar one,

$$\Omega = M \int \frac{dt}{\sqrt{t^2-1}} + N$$

$$= M \cosh^{-1} t + N$$

or

$$t = \cosh \frac{\Omega - N}{M}$$

The values of M, N, f, and g can now be evaluated. At C, $t = 1$ and $\Omega = -i\pi/2 = N$. At B, $t = -1$ and $\Omega = 0$, so that

$$\frac{i\pi}{2M} = \cosh^{-1}(-1) = -i\cos^{-1}(-1) = \pm i\pi$$

and $M = 1/2$, the positive sign being selected. Once M and N are

known. f and g can be evaluated by substituting $\ln (V_0/V_j)$ and $-i\beta$, respectively, for Ω.

$$f = -\cosh\left(\ln \frac{V_0^2}{V_j^2}\right) = -\frac{1}{2}\left(\frac{V_0^2}{V_j^2} + \frac{V_j^2}{V_0^2}\right)$$

$$g = -\cos 2\beta$$

The equation relating w and t can be obtained as before, or directly from the known complex function for the source and sink

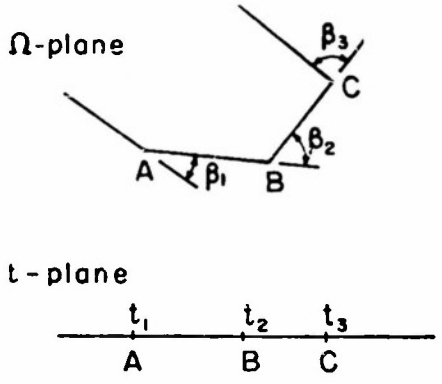

FIG. 5. PLANES FOR SCHWARZ-CHRISTOFFEL TRANSFORMATION.

in the t-plane. In the first instance the Schwarz-Christoffel transformation leads to the form

$$w = M' \int \frac{dt}{(t-f)(t-g)} + N'$$

The final form is, however, obtained without integration if it is noted that $V_0 b$, the quantity of flow in the z-plane is just half the strength of the source at A and of the sink at D in the t-plane. Thus,

$$w = -\frac{V_0 b}{\pi}\left[\ln(t-f) - \ln(t-g)\right]$$

In cases such as this one, in which the entire boundary in the hodograph plane coincides with the boundary of a circular sector, a direct transformation from the ζ-plane to the w-plane is possible [13]. For the elementary example herein, this relationship can be obtained by the simple expedient of constructing the image pattern

of the source and sink in the x- and y-axes and in the circular boundary as shown in Fig. 6. The resulting expression for $w(\zeta)$ with a term for each of the four sources and four sinks will lead to a relationship equivalent to that obtained by the method outlined first. Alternatively, the ζ- and t-planes are simply connected by means of the relationship

$$t = \frac{1}{2}\left(\frac{\zeta^2}{V_j^2} + \frac{V_j^2}{\zeta^2} \right)$$

Which planes and which methods are appropriate in a given case depends upon the type of problem and the nature of the calculation to be made.

Once $w(t)$ and either $\Omega(t)$ or $\zeta(t)$ have been defined, the desired function $w(z)$ is implicitly defined, both Ω and ζ being expressible in terms of dw/dz. If the resulting ordinary differential equations

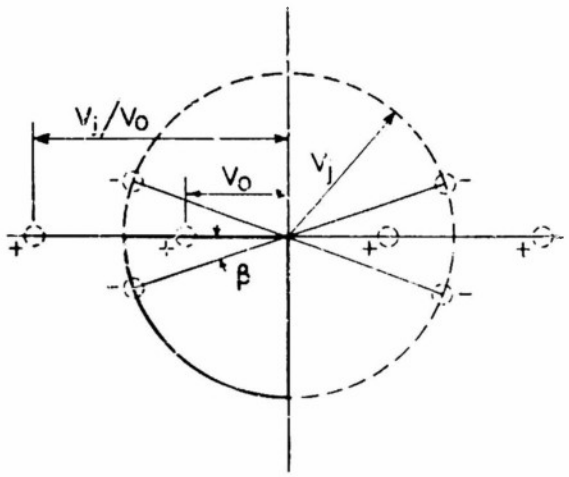

FIG. 6. IMAGE PATTERN FOR CIRCULAR QUADRANT.

can be integrated, three kinds of results can be obtained: (1) parametric equations relating bulk characteristics, i.e., a/b, V_0, and β, in the foregoing example, (2) the profile of the jet, and (3) the variation of velocity and pressure along the solid boundaries. Such calculations are presented in some detail in each of the following papers. In addition, a still more complicated result, which usually requires numerical integration, is available in that ϕ or ψ can be defined at any point in the region of flow in the z-plane.

APPLICABILITY OF METHOD

From the mathematical viewpoint, the direct calculation of free-streamline flows is restricted to two-dimensional irrotational flows of incompressible fluids which are free from gravitational effects and for which the solid boundaries are straight. As flows of real fluids seldom satisfy fully these stringent restrictions, the practical value of the results is open to question. The significance of the various restrictions can be shown only by comparing the calculated results with those obtained from observations of real flows.

The importance of viscous effects, or of relatively small departures from irrotational flow, has already been studied in detail for various kinds of flow. It is well known that for flows in which shear is not a primary factor, such as rapidly accelerated flows, the differences between comparable ideal and real fluid flows are small.

In many problems the importance of gravitational effects is already known to be definitely secondary. For example, the coefficient of contraction for an orifice in a vertical wall does not differ significantly from that for one in a horizontal wall, even though the attraction of the earth affects the trajectories for the two cases in quite different ways. On the contrary, for flows in which a free surface has a significant bearing on the flow pattern, as in flow over a weir, the conventional methods are no longer adequate.

The presence of curved solid boundaries leads to calculations which are both extremely complex in detail and indirect in application. The ζ-plane is no longer directly useful, and the Ω-plane contains lines which are either slanting or curved. The transformation between Ω and t thus becomes more complicated, even if definable, and the calculation can usually proceed only if the form of the boundary in the Ω-plane is assumed first and the corresponding physical boundary in the z-plane is derived therefrom. As the latter boundary may not be useful or even significant, a tedious trial-and-error calculation will be required for the solution of any given curved boundary.

The applicability to axisymmetric flows of the results computed for plane flows can be assessed only by the making of suitable comparisons as in references [5] and [12] and in the following papers. Comparisons have been made both between results of theory and experiment, on the one hand, and between two dimensional

and axisymmetric flows, on the other. Already at hand is convincing evidence of a surprisingly close correspondence between these two classes of flows, at least insofar as certain bulk characteristics are concerned. Even in cases for which differences have been noted, the extensive results which are available for two-dimensional flows are useful in indicating trends to be expected for comparable axisymmetric and three-dimensional flows.

Among the various types of two-dimensional flow patterns which can be analyzed as free-streamline flows are free efflux, deflection of jets, and various combinations of the two. Efflux patterns have been calculated for a variety of boundary geometries including those for infinitely large reservoirs and for slots at the ends of conduits with various boundary configurations. For jets impinging on flat plates, the characteristics of flow have been determined for finite and infinite extents of fluid, for free and partially bounded jets, and for deflectors of various proportions (each being composed of necessarily straight-line segments). In another type of calculation the free streamline has been used as an indication of the configuration of cavities in fluid flows.

Additional calculations of these several kinds of flows, presented in the following papers, include characteristic results which are useful for the interpretation of real fluid flows. The calculations provide information for specific designs; comparisons between results of theory and of observation serve to indicate the applicability of the method.

TRANSITION CURVES OF CONSTANT PRESSURE
I. STREAMLINED STRUTS

by
R. GERBER* and JOHN S. McNOWN

Transition curves along which the pressure is an arbitrarily assigned constant can be obtained for two-dimensional flows by means of an adaptation of the Helmholtz-Kirchhoff theory for free streamlines. These curves can be used in the determination of the profile of the upstream portion of streamlined struts or piers so as to reduce negative pressures and prevent marked adverse pressure gradients. Consequently, the likelihood of occurrence of either cavitation or separation can be significantly diminished. Although the results of such calculations are immediately applicable only to two-dimensional flow of incompressible fluids, the scope of the application is less restricted than it would appear. The bulk characteristics of certain free-streamline flows have been found to be essentially the same for two-dimensional and axisymmetric patterns. Also, the criteria for reduction of shock-waves in compressible fluids have been found to parallel closely those for the reduction of cavitation, making possible the use of such results in compressible flows. The calculation described herein was suggested by Professor Kravtchenko of the Faculté des Sciences at the University of Grenoble.

A series of symmetrical profiles which are suitable for transition curves, and which are at the same time readily calculable, can be obtained for the flow pattern shown in Fig. 1a. A flat plate CC' normal to the direction of the uniform flow at infinity is connected to linear boundaries such as DE paralleling the direction of flow by curves such as CD which are not defined geometrically but along which the velocity is equal to an arbitrarily selected constant. This constant velocity V_1 is greater than the velocity at infinity V_0, the problem reducing to the classical problem of the infinite cavity [14] if V_1 is equal to V_0. Considering only the upper half of the symmetrical flow pattern, one finds that the direction of flow is

*Assistant, Department of Mathematics, University of Grenoble, France.

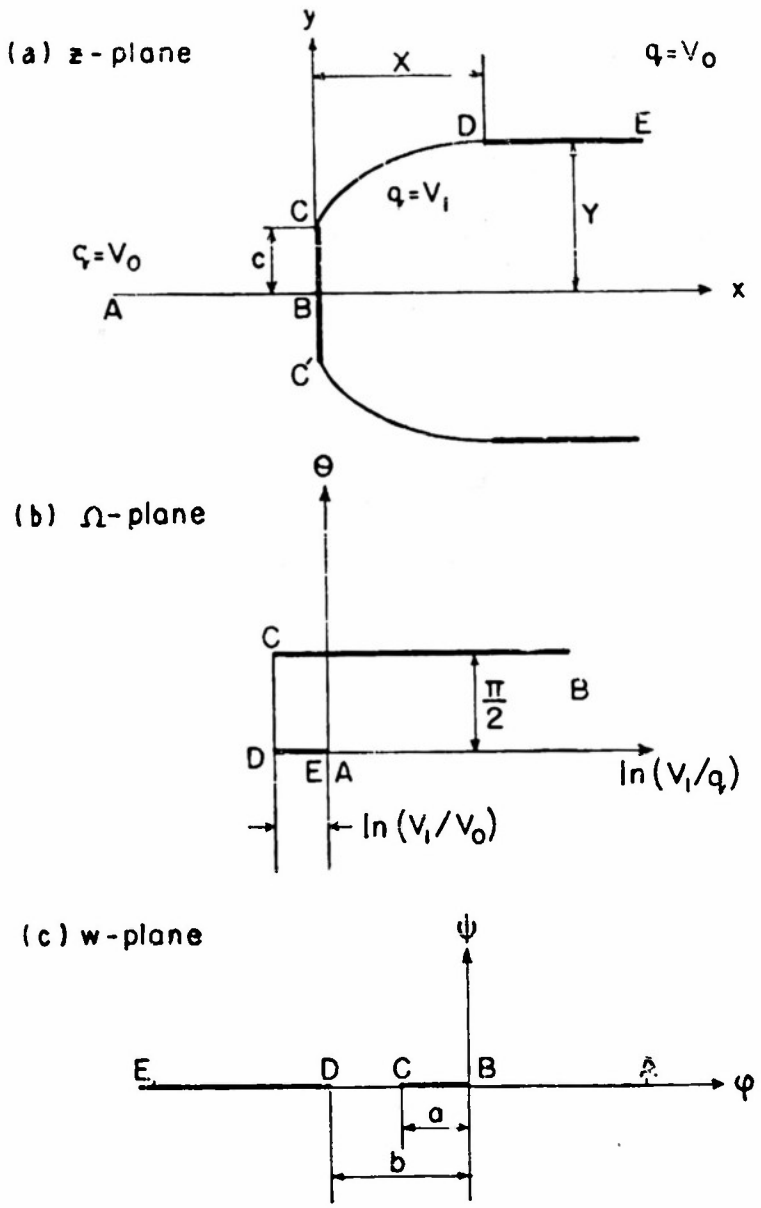

FIG. 1. CONFORMAL-MAPPING PLANES.

a known constant along the segments AB, BC, and DE, and that along the remaining segment CD the velocity magnitude is constant. Thus, the necessary requirements for the application of the free-streamline theory are fulfilled.

From the mathematical point of view, the problem reduces to the determination of the complex function relating the velocity potential and the stream function to the desired flow pattern by means of an intermediate stage which is a logarithmic hodograph.

If the complex potential is designated as $w = \phi + i\psi$, the complex velocity can be represented by the expression:

$$-\frac{dw}{dz} = u - iv = V_0 e^{-\Omega} \tag{1}$$

in which $\Omega = -\ln(q/V_0) + i\theta$ is defined in terms of the direction and magnitude of the vector velocity. The inclination of the velocity to the x-axis is θ, and the velocity magnitude is q. The boundary streamline is a semi-infinite rectangle in the Ω-plane, Fig. 1b, and, of course, a straight line in the w-plane, Fig. 1c.

The transforming function between w and Ω can be obtained directly by means of the Schwarz-Christoffel theorem. After integration and evaluation of constants,

$$\Omega = \frac{i}{2}\cos^{-1}\frac{m(w+K)}{w} - \frac{1}{2}\cosh^{-1} m \tag{2}$$

in which m is defined by the relationships (see Fig. 1c),

$$b = \frac{Km}{m-1} \quad , \quad a = \frac{Km}{m+1} \qquad (m>1)$$

and K is a constant having the same dimensions as w. Along the arc CD,

$$\ln\frac{V_1}{V_0} = \frac{1}{2}\cosh^{-1} m$$

so that

$$m = \frac{1}{2}\left[\left(\frac{V_1}{V_0}\right)^2 + \left(\frac{V_0}{V_1}\right)^2\right] \tag{3}$$

Completion of the analysis consists of the algebraic definition of the transition curves as a function of the assigned velocity ratios. In other words, x/c and y/c (Fig. 1a) are to be expressed as functions of V_1/V_∞, or m. Because $q = v = -\partial\phi/\partial y$ along BC, the reference length c can be defined in integral form,

$$c = \int_0^c dy = -\int_0^a \frac{d\phi}{v} \tag{4}$$

From Eq. (2) it can be shown that

$$v = V_1 \exp\left[-\frac{1}{2}\cosh^{-1}\frac{m(\phi+K)}{\phi}\right]$$

whereby $d\phi$ can be expressed in terms of v. If, in addition, the substitution $t = V_1/v$ is made,

$$c = \frac{4mK}{V_1}\int_0^\infty \frac{(t^4-1)t^2}{(t^4+2mt^2+1)^2}\,dt$$

$$= \frac{K}{V_1}\frac{V_1^4+V_0^4}{V_1^4-V_0^4}\left[\frac{V_1^2-V_0^2}{V_1^2+V_0^2}+\frac{V_1}{V_0}\tan^{-1}\frac{V_1}{V_0}-\frac{V_0}{V_1}\tan^{-1}\frac{V_0}{V_1}\right] \tag{5}$$

Along the arc CD, the relationships between ϕ, θ, and the coordinates x and y are well known:

$$V_1\,dx = -\cos\theta\,d\phi$$

$$V_1\,dy = -\sin\theta\,d\phi$$

Also, from Eq. (2),

$$\cos 2\theta = \frac{m(\phi+K)}{\phi} \qquad \left(-\frac{m}{m+1} < \phi < \frac{m}{m-1}\right)$$

After substitution and integration, parametric equations for the curve are obtained in the following form:

$$x = \frac{mK}{2V_1}\left[\frac{\cos\theta}{\frac{m+1}{2}-\cos^2\theta}-\sqrt{\frac{2}{m+1}}\tanh^{-1}\left(\sqrt{\frac{2}{m+1}}\cos\theta\right)\right] \tag{6}$$

$$y = c + \frac{mK}{2V_1}\left[\frac{\sin\theta}{\frac{m-1}{2}+\sin^2\theta}-\frac{2}{m-1}\right.$$

$$\left.+\sqrt{\frac{2}{m-1}}\left\{\tan^{-1}\sqrt{\frac{2}{m-1}}-\tan^{-1}\left(\sqrt{\frac{2}{m-1}}\sin\theta\right)\right\}\right]$$

The values for the coordinates of point B (X and Y in Fig. 1a) are obtained from Eq. (6) if the value of zero is substituted for θ:

$$X = \frac{mK}{2V_1}\left[\frac{2}{m-1}-\sqrt{\frac{2}{m+1}}\tanh^{-1}\sqrt{\frac{2}{m+1}}\right]$$

$$Y = c + \frac{mK}{2V_1}\left[\sqrt{\frac{2}{m-1}}\tan^{-1}\sqrt{\frac{2}{m-1}}-\frac{2}{m-1}\right] \tag{7}$$

Finally, the parameter m, which has been defined in terms of V_1/V_0, can be expressed in terms of the dimensionless pressure change σ,

$$\sigma = \frac{p_0-p_1}{\rho V_0^2/2} \tag{8}$$

which is equivalent to the cavitation number if p_1 equals the vapor pressure. The relationship between m and σ is as follows.

$$m = \frac{1}{2}\left[1 + \sigma + \frac{1}{1+\sigma}\right] \tag{9}$$

Results of calculations based on Eqs. (6) and (7) are shown in Fig. 2. The solid lines indicate the shape of the free streamlines for σ-values of 0.4 and 0.7. The broken line is the locus of the downstream end of the curved portion, that is, it indicates the relationship between Y/c and X/c. On the latter curve representative values of σ are shown, those for 0.4 and 0.7 corresponding, of

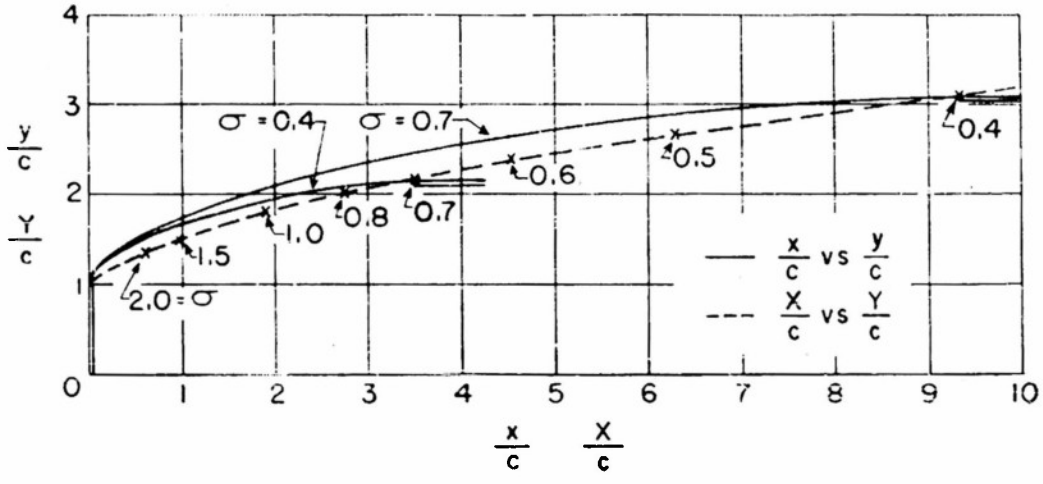

FIG. 2. CHARACTERISTIC TRANSITION CURVES WITH LOCUS OF TERMINAL POINTS.

course, with the downstream ends of the transition curves calculated. It is known that both the length and the width of the cavity approach infinity as σ approaches zero, and it can be shown from Eq. (7) that X approaches Y and that both approach zero as σ approaches infinity. From the practical viewpoint, however, the occurrence of separation prevents the attainment of flows comparable to σ-values greater than approximately 0.5, a point discussed by Birkhoff [13].

Although marked differences exist between results of computations based on two-dimensional flows and observations of otherwise comparable three-dimensional flows, remarkably close comparisons have been found between certain bulk characteristics [6,12,15]. Whereas the profiles of free streamlines are markedly different, the ratios of comparable areas have been found to be the same for the two kinds of flow, an observation which led the writers

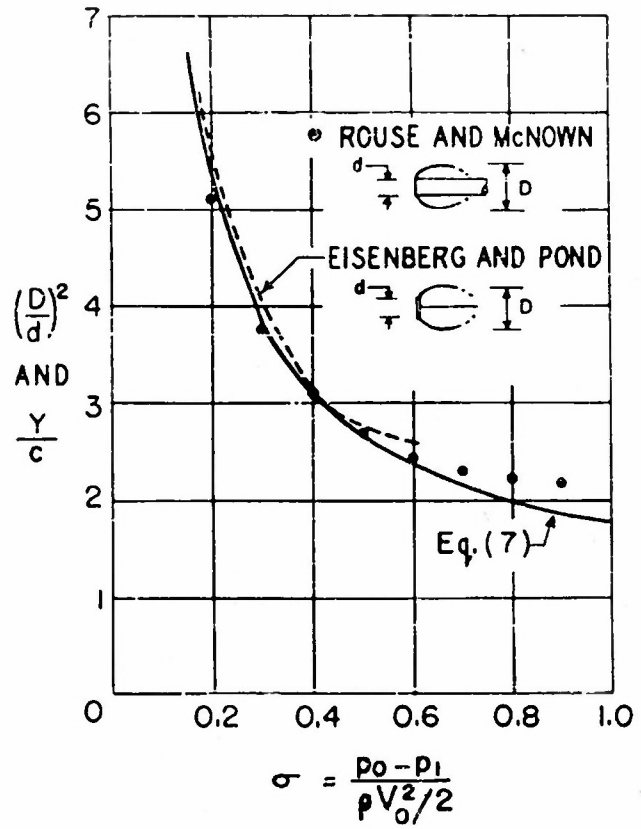

FIG. 3. COMPARISON OF RATIOS CALCULATED FOR TWO-DIMENSIONAL FLOW WITH THOSE MEASURED FOR AXISYMMETRIC FLOWS.

to make a similar comparison of the Y/c-values with the ratios of the area of a plate or a disk to the measured cross section of cavitation pockets they cause to form in axisymmetric flows. The comparison between the results obtained from Eq. (7) and the observations made in the water tunnels of the Iowa Institute of Hydraulic Research [16] and of the David Taylor Model Basin [17] is shown in Fig. 3. Surprisingly good correspondence is obtained for small values of σ; the effect of separation is evident in the discrepancies occurring for σ greater than 0.6. The agreement obtained is better than that which Eisenberg [18] found in a similar comparison with the theory of Riabouchinsky and that of Gilbarg and Rock, but the reason for this improvement is not evident.

In conclusion, the writers believe that the calculation of the irrotational flow patterns herein presented is directly applicable in certain design problems, that it can be extended or modified to describe other related flows, and that certain applications are possible for axisymmetric flows.

TRANSITION CURVES OF CONSTANT PRESSURE
II. INLETS

by

D. W. Appel and E. M. Laursen*

Patterns of flow through well streamlined contractions have been found to be defined at least moderately well by potential-flow theory. The particular type of contraction transition to be considered herein is characterized by a constant pressure (and therefore a constant magnitude of velocity) along the curved portion of the boundary. This type of transition for two-dimensional flows is amenable to free-streamline analysis provided that the boundaries upstream and downstream from the constant-pressure section are made up of straight lines, along which the direction of the flow is constant. The form of the curved boundary thus should be calculable by the free-streamline techniques outlined in the first paper of this bulletin and the problem is an extension of that in the preceding paper.

Several advantages are inherent in this constant-pressure transition. The minimum pressure in the transition, that along the free streamline, can be specified; thus, the likelihood of cavitation can be directly controlled. Since there is no adverse pressure gradient within the curved portion of the transition, the probability of a separation of the flow from the boundary is also reduced. Finally, the occurrence of the maximum velocity all along the free streamline should result in a minimum size for the transition.

The location of the boundaries of a general two-dimensional contraction are shown in Fig. 1a. For an infinite value of the upstream width, the figure represents one half of a symmetrical inlet from an infinite reservoir. For upstream widths greater than the downstream, the figure represents various degrees of contraction of two-dimensional flow. If the centerline and the upstream boundary are considered to be repeating lines of symmetry, the figure represents either the upstream portion of a series of struts, or,

*Research Associate and Research Engineer, respectively, Iowa Institute of Hydraulic Research, State University of Iowa, Iowa City.

conversely, a series of equidistant inlets from an infinite reservoir. The equation to be derived for the form of the constant-pressure transition can be applied in studies of flow past any of these boundary forms.

MATHEMATICAL ANALYSIS

The four planes described in the introductory paper and used in the following analysis of two-dimensional flow contractions are shown in Fig. 1. In the flow plane (the z-plane), the reference

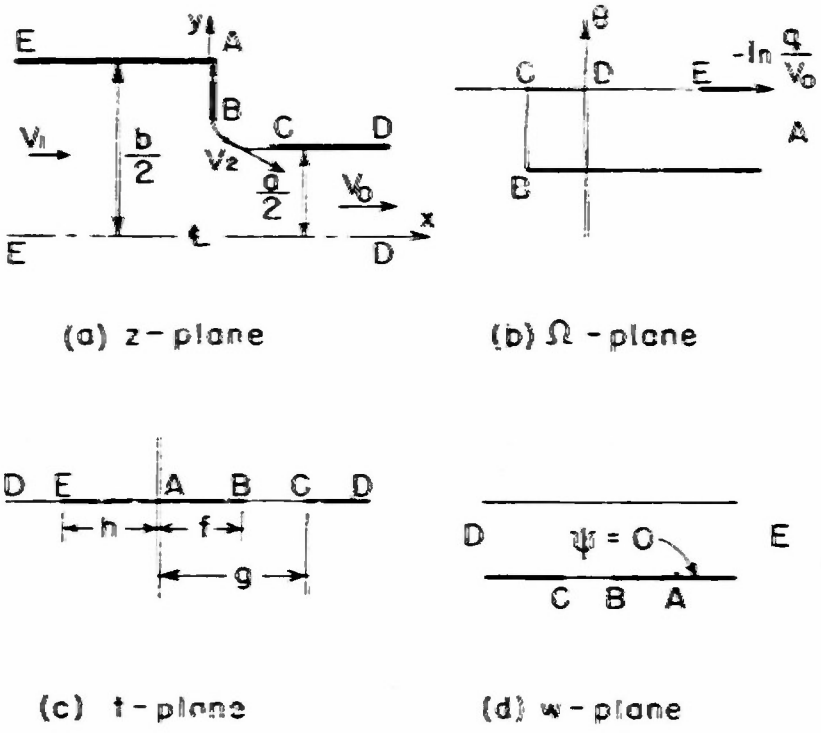

FIG. 1. TRANSFORMATION PLANES.

velocities along the boundary are shown. The flow is represented in the logarithmic hodograph (the Ω-plane) by the usual relationship,

$$\Omega = -\ln \frac{q}{V_0} + i\theta \tag{1}$$

for which the bounding streamlines take the form of a semi-infinite rectangle. The open end of the rectangle at infinity corresponds to the stagnation point A, and the two 90° vertices correspond to points B and C at each end of the free streamline.

By means of the Schwarz-Christoffel theorem the semi-infinite rectangle in the Ω-plane is mapped onto one-half of the auxiliary

t-plane. Points A and D are arbitrarily placed at zero and infinity in the t-plane. Rather than to fix [illegible] point in the t-plane, it is convenient to relate the distances f and g by the parametric equations

$$f = \frac{m}{m+1} \quad , \quad g = \frac{m}{m-1} \qquad (m>1)$$

The Schwarz-Christoffel transformation between the Ω-plane and the t-plane is then

$$\Omega = -\ln \frac{V_2}{V_0} + \frac{i}{2}\cos^{-1}\left[\frac{m(t-1)}{t}\right] \tag{2}$$

The constants in the transformation were evaluated by substitution of the values of Ω and t for points A and B in the two planes. An equation for the parameter m can be obtained by substituting values of Ω and t for the point D in the two planes, whence

$$m = \frac{1}{2}\left[\left(\frac{V_2}{V_0}\right)^2 + \left(\frac{V_0}{V_2}\right)^2\right]$$

Thus, if the velocity along the transition V_2 relative to the velocity in the downstream channel V_0 is specified, m is determined.

The infinite rectangle representing the potential and stream functions in the w-plane is mapped onto the lower half of the t-plane by the transformation

$$w = \phi + i\psi = -\frac{V_0 a}{2\pi}\ln(t+k) \tag{3}$$

This equation can be derived by means of the Schwarz-Christoffel theorem or from the expression for a source located at point E. The evaluation of Eq. (2) for the point E gives an expression for k,

$$k = \frac{n}{n-m}$$

in which n is determined by the ratio of the free-streamline velocity V_2 to the upstream channel velocity V_1 according to the equation

$$n = \frac{1}{2}\left[\left(\frac{V_2}{V_1}\right)^2 + \left(\frac{V_1}{V_2}\right)^2\right]$$

If the restriction that the magnitude of the variable velocity q equals that of V_2 is imposed, parametric differential equations for the free-streamline can be obtained. Equation (1) thus becomes, for the free streamline,

$$\Omega = -\ln \frac{V_2}{V_0} + i\theta \tag{4}$$

Simultaneous solution of Eqs. (2), (3), and (4) gives the following relationship between the complex potential w and the inclination of the free streamline θ:

$$w = \phi + i\psi = -\frac{V_0 a}{2\pi} \ln \left[\frac{m}{m - \cos 2\theta} + \frac{m}{n-m} \right] \tag{5}$$

For convenience the free streamline has been taken as $\psi = 0$. The distance s along the free streamline from B to a point at which the inclination is θ can be obtained by combining the equation defining the velocity, $\partial\phi/\partial s = -V_2$, with Eq. (5), and integrating:

$$s = \frac{V_0 a}{2\pi V_2} \ln \left[\frac{m}{m - \cos 2\theta} + \frac{m}{n-m} \right] \tag{6}$$

Because s is the curvilinear distance along the bounding streamline, this expression is not directly useful for obtaining the profile of the transition. However, the equation can be expressed in rectangular coordinates through the differential relationships

$$dx = ds \cos\theta \quad , \quad dy = ds \sin\theta$$

The parametric differential equations for the curved boundary are then

$$dx = -2 \frac{V_0}{V_2} \frac{a}{\pi} (m-n) \left[\frac{\cos^2\theta \; d(\cos\theta)}{(m+1-2\cos^2\theta)(n+1-2\cos^2\theta)} \right] \tag{7}$$

and

$$dy = -2 \frac{V_0}{V_2} \frac{a}{\pi} (m-n) \left[\frac{\sin^2\theta \; d(\sin\theta)}{(m-1+2\sin^2\theta)(n-1+2\sin^2\theta)} \right] \tag{8}$$

Fortunately these equations are readily integrable; one obtains the parametric equations

$$\frac{x}{a} = \frac{1}{\pi} \frac{V_0}{V_2} \left[\sqrt{(m+1)/2} \tanh^{-1} \frac{\cos\theta}{\sqrt{(m+1)/2}} - \sqrt{(n+1)/2} \tanh^{-1} \frac{\cos\theta}{\sqrt{(n+1)/2}} \right] \tag{9}$$

and

$$\frac{y}{a} = \frac{1}{2} + \frac{1}{\pi} \frac{V_0}{V_2} \left[\sqrt{(n-1)/2} \tan^{-1} \frac{\sin\theta}{\sqrt{(n-1)/2}} - \sqrt{(m-1)/2} \tan^{-1} \frac{\sin\theta}{\sqrt{(m-1)/2}} \right] \tag{10}$$

if the origin of x and y is chosen such that $x = 0$ if $\theta = -\pi/2$ and $y = a/2$ if $\theta = 0$. Equation (9) can be written in an alternative logarithmic form.

$$\frac{x}{a} = \frac{1}{2\pi}\frac{V_0}{V_2}\left[\sqrt{(m+1)/2}\,\ln\frac{\sqrt{(m+1)/2}+\cos\theta}{\sqrt{(m+1)/2}-\cos\theta} - \sqrt{(n+1)/2}\,\ln\frac{\sqrt{(n+1)/2}+\cos\theta}{\sqrt{(n+1)/2}-\cos\theta}\right]$$

For the case of the infinite reservoir in which $n = \infty$, Eqs. (9) and (10) can be reduced to

$$\frac{x}{a} = \frac{1}{\pi}\frac{V_0}{V_2}\left[\sqrt{(m+1)/2}\,\tanh^{-1}\frac{\cos\theta}{\sqrt{(m+1)/2}} - 2\cos\theta\right] \quad (11)$$

and

$$\frac{y}{a} = \frac{1}{2}+\frac{1}{\pi}\frac{V_0}{V_2}\left[\sin\theta - \sqrt{(m-1)/2}\,\tan^{-1}\frac{\sin\theta}{\sqrt{(m-1)/2}}\right] \quad (12)$$

after evaluation of the indeterminate forms. Réthy in 1893 [19] presented equations similar in form to Eqs. (9) and (10). However, his equations were based upon parameters which could not be directly evaluated from the flow characteristics.

Upstream and downstream from the curved boundary the magnitude of the velocity is variable, but the direction of the velocity along the boundary is known. Equations (1), (2), and (3) can be used to obtain the velocity distribution along the straight portions of the boundary by steps essentially parallel to those used for the calculation of the free-streamline profile. For the general case, the velocity distribution can be obtained from the equation

$$\frac{x}{a} = \frac{d}{a}+\frac{2}{\pi}(m-n)\left[K_1\left(\tanh^{-1}\frac{qV_0}{V_2^2}-\tanh^{-1}\frac{V_0}{V_2}\right) + K_2\left(\tanh^{-1}\frac{V_0}{q}-\tanh^{-1}\frac{V_0}{V_2}\right) - K_3\left(\tanh^{-1}\frac{qV_1}{V_2^2}-\tanh^{-1}\frac{V_1}{V_2}\right) + K_4\left(\tanh^{-1}\frac{V_1}{q}-\tanh^{-1}\frac{V_1}{V_2}\right)\right] \quad (13)$$

downstream from the transition, and

$$\frac{y}{a}=\frac{1}{2}+\frac{c}{a}+\frac{2}{\pi}(m-n)\left[K_1\left(\tan^{-1}\frac{qV_0}{V_2^2}-\tan^{-1}\frac{V_0}{V_2}\right)\right.$$
$$+K_2\left(\tan^{-1}\frac{q}{V_0}-\tan^{-1}\frac{V_2}{V_0}\right)$$
$$+K_3\left(\tan^{-1}\frac{qV_1}{V_2^2}-\tan^{-1}\frac{V_1}{V_2}\right)$$
$$\left.+K_4\left(\tan^{-1}\frac{q}{V_1}-\tan^{-1}\frac{V_2}{V_1}\right)\right] \qquad (14)$$

upstream from the transition. In Eqs. (13) and (14),

$$K_1=[(V_2/V_0)^2-(V_2/V_1)^2]^{-1}\,[(V_2/V_0)^2-(V_1/V_2)^2]^{-1}$$
$$K_2=(V_0/V_2)^2\,[(V_0/V_2)^2-(V_2/V_1)^2]^{-1}\,[(V_0/V_2)^2-(V_1/V_2)^2]^{-1}$$
$$K_3=(V_0/V_1)\,[(V_2/V_1)^2-(V_2/V_0)^2]^{-1}\,[(V_2/V_1)^2-(V_0/V_2)^2]^{-1}$$
$$K_4=(V_0V_1/V_2^2)\,[(V_1/V_2)^2-(V_2/V_0)^2]^{-1}\,[(V_1/V_2)^2-(V_0/V_2)^2]^{-1}$$

and c and d are the dimensions of the transition. The form of these equations for the special case of the infinite reservoir is

$$\frac{x}{a}=\frac{d}{a}-\frac{1}{\pi}\frac{V_0}{V_2}\left[1-\frac{V_2}{q}\right]+\frac{1}{\pi}\left(\frac{V_0}{V_2}\right)^2\left[\tanh^{-1}\frac{qV_0}{V_2^2}-\tanh^{-1}\frac{V_0}{V_2}\right]$$
$$+\frac{1}{\pi}\left[\tanh^{-1}\frac{V_0}{q}-\tanh^{-1}\frac{V_0}{V_2}\right] \qquad (15)$$

downstream from the transition, and

$$\frac{y}{a}=\frac{1}{2}+\frac{c}{a}-\frac{1}{\pi}\frac{V_0}{V_2}\left[1-\frac{V_2}{q}\right]+\frac{1}{\pi}\left(\frac{V_0}{V_2}\right)^2\left[\tan^{-1}\frac{qV_0}{V_2^2}-\tan^{-1}\frac{V_0}{V_2}\right]$$
$$+\frac{1}{\pi}\left[\tan^{-1}\frac{q}{V_0}-\tan^{-1}\frac{V_2}{V_0}\right] \qquad (16)$$

upstream from the transition. The pressure distribution can be obtained directly by means of the Bernoulli theorem.

Particular constant-pressure transitions can now be calculated for specified values of the velocity ratios V_2/V_0 and V_2/V_1, or, what is equivalent, for specified values of the minimum pressure along the transition and the contraction ratio b/a. In order to make

the results of sample calculations general, values of a dimensionless pressure parameter σ have been assumed and the corresponding pressures calculated from the definition equation,

$$\sigma = \frac{p_0 - p_2}{\rho V_0^2/2} \tag{17}$$

If p_2 is the vapor pressure, σ is the familiar cavitation index. Since the pressure and velocity are related by the Bernoulli equation, the velocity ratio V_2/V_0 can also be obtained from the equivalent expression

$$\sigma = \left(\frac{V_2}{V_0}\right)^2 - 1$$

Transition profiles have been calculated for a value of σ of 0.4 and contraction ratios b/a of ∞, 4, and 2. The profiles are shown

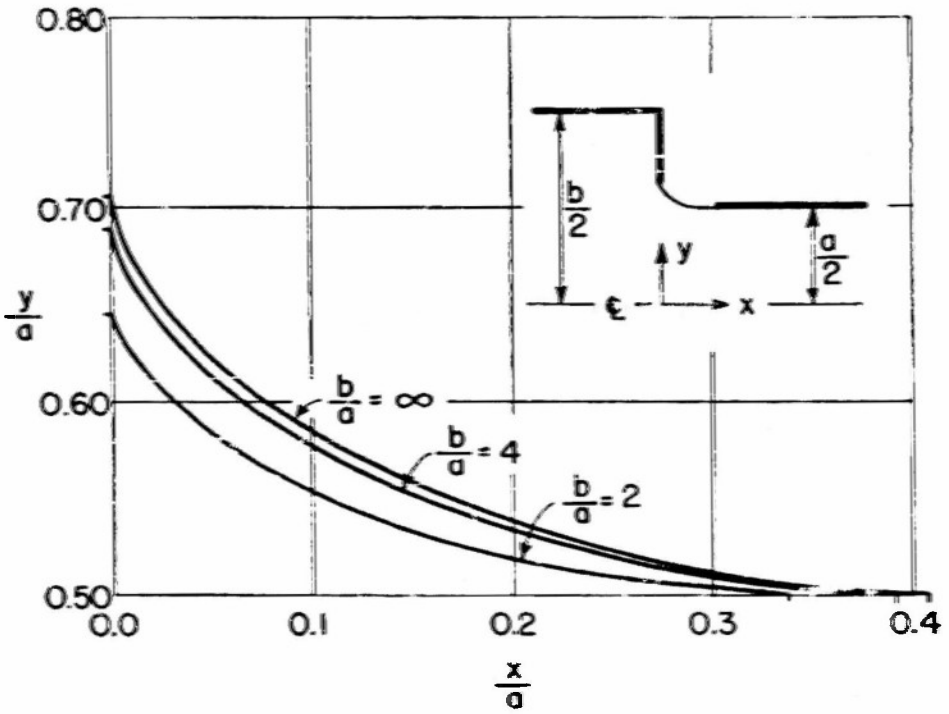

FIG. 2. TRANSITION PROFILES FOR A CONSTANT PRESSURE INDEX OF $\sigma = 0.4$.

in Fig. 2. For different values of σ, the two principal dimensions of the transition, the length d and the width c, are shown in Fig. 3. As σ approaches zero, i.e., as $V_2 \rightarrow V_0$, the length of the transition approaches infinity.

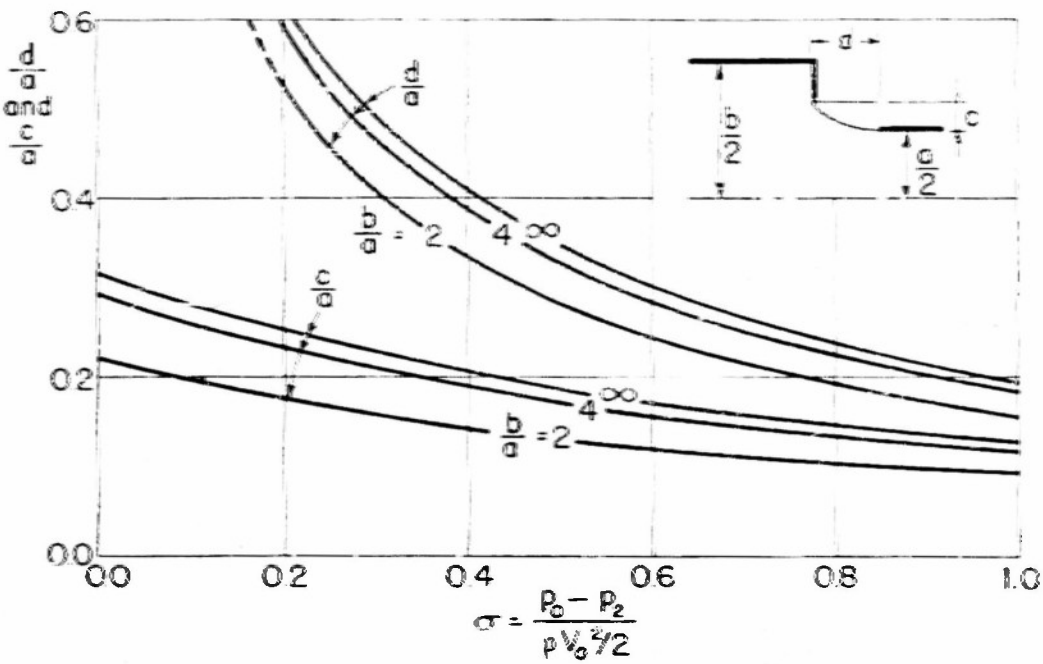

FIG. 3. CONSTANT-PRESSURE TRANSITION DIMENSIONS.

COMPARISON BETWEEN RESULTS OF THEORY AND EXPERIMENT

In 1917, von Mises [4] published an expression for the contraction coefficient for free efflux corresponding to $V_2 = V_3$ in the above analysis. Equation (10) for $w = 1$ and $\theta = -\pi/2$, if expressed in terms of a contraction coefficient, is found to be identical to von Mises' equation:

$$\frac{1}{C_c} = 1 + \frac{2c}{a} = 1 + \frac{2}{\pi}\left[\frac{1}{2}\left(\frac{b}{a} - \frac{a}{b}\right)\right] \cot^{-1}\left[\frac{1}{2}\left(\frac{b}{a} - \frac{a}{b}\right)\right] \quad (18)$$

Although von Mises did not compute the jet profile, he used the free-streamline theory to obtain the pressure distribution on the channel walls. With knowledge of the pressure distribution, he obtained the contraction coefficient by means of the equation of momentum. Since von Mises' equation is a limit to the theoretical expressions obtained herein, observed agreement between the results of experiments and his computed coefficients is a partial verification of the present analysis.

In order to test the performance of the theoretical transition forms in detail, experiments were conducted with air flow through

half models of two of the profiles shown in Fig. 2 ($b/a = \infty$ and $b/a = 2$). The curved boundary and portions of the straight boundary upstream and downstream were made of Lucite with piezometric taps along the centerline. The width $a/2$ was 9.2 inches and the height was also 9.2 inches, making the downstream cross section square. The flow of air was produced and controlled by a variable-discharge blower located seven feet downstream from the transition section. The rate of flow was determined by means of a calibrated nozzle on the discharge side of the blower.

The theoretical pressure distribution along the boundary of the inlet from the infinite reservoir is shown in Fig. 4a along with test results for downstream conduit velocities of 17 and 46 fps, corresponding to Reynolds numbers of 75,000 and 200,000 based on the half-width of 9.2 inches. An approximately constant pressure was obtained along the curved boundary for both tests. The greater reduction in pressure for the higher velocity indicates a trend toward the theoretical value for $\sigma = 0.4$ with increasing Reynolds number. That viscous effects result in a higher pressure is noteworthy, because the design thus tends to be conservative

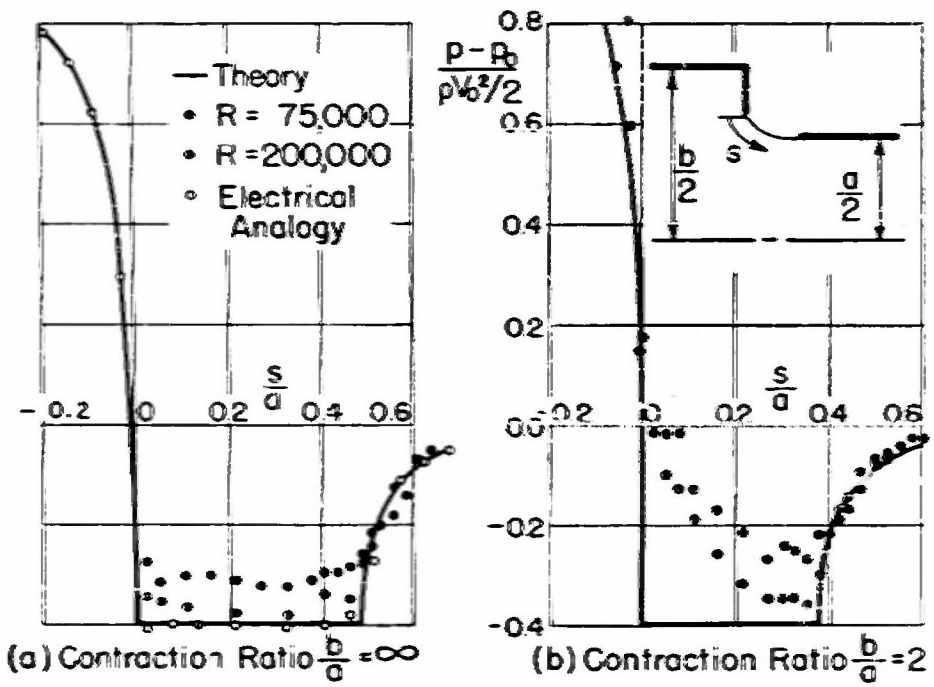

FIG. 4. PRESSURE DISTRIBUTIONS OBTAINED ALONG BOUNDARIES OF DERIVED TRANSITION FORMS.

and the likelihood of cavitation tends to be even less than anticipated.

The pressure distribution along the boundary for the 2:1 channel contraction is shown in Fig. 4b for the same Reynolds numbers as above. The velocity distribution in the upstream channel evidently affects the pressure distribution so that the pressure along the transition boundary is not constant and the minimum pressure occurs near the downstream end of the transition. Again the trend is to approach the theoretical pressure reduction at higher Reynolds numbers. However, the eddy which forms near the right angle at the beginning of the contraction would probably affect the pressure distribution regardless of the Reynolds number.

COMPARISON WITH OTHER TRANSITION FORMS

Figure 4a also shows the results of a test that was made on a model of one of the constant-pressure transitions in an electrical-analogy tank. Since the electrical-analogy method is based on the same assumption of potential flow as is implicit in the free-streamline analysis, the excellent agreement with the theoretical pressure distribution simply verifies the technique and accuracy of the electrical-analogy method. However, the check allows the results of tests (as yet unpublished) on circular and elliptical transitions to be used with confidence in the comparison of transition dimensions shown in Fig. 5. Although the data available from the electrical-analogy experiments are limited to a few shapes and to inlets from an infinite reservoir, the surmise that the dimensions of the constant-pressure transition are the smallest possible for a given minimum pressure along the boundary is upheld.

In other studies certain bulk characteristics of axisymmetric flow have been found to be essentially the same as those of two-dimensional free-streamline flow. Two additional electrical-analogy tests were run to investigate the theoretical performance of the two-dimensional free-streamline profile as an axisymmetric transition. In one test the calculated profile for $\sigma = 0.4$ was used, i.e., $r/r_0 = y/(\sigma/2)$. The dimensionless pressure parameter at the beginning of the curved boundary was positive and decreased to about ¾ of the theoretical value of -0.4 close to the end of the transition. The higher pressures were probably due in part to the larger relative area at each section. In the second test the profile

was modified to have the same relative area at any section, i.e.,

$$\frac{r}{r_0} = \sqrt{\frac{y}{a/2}}$$

A very large negative pressure, four times the theoretical, resulted at the beginning of the curve, with a rise to about one-half the theoretical in the last half of the transition. The large negative pressure at the beginning of the transition is probably due to the considerable curvature at this point. That both the area of flow and the boundary curvature are important in determining the pressure along the boundary is apparent from these results.

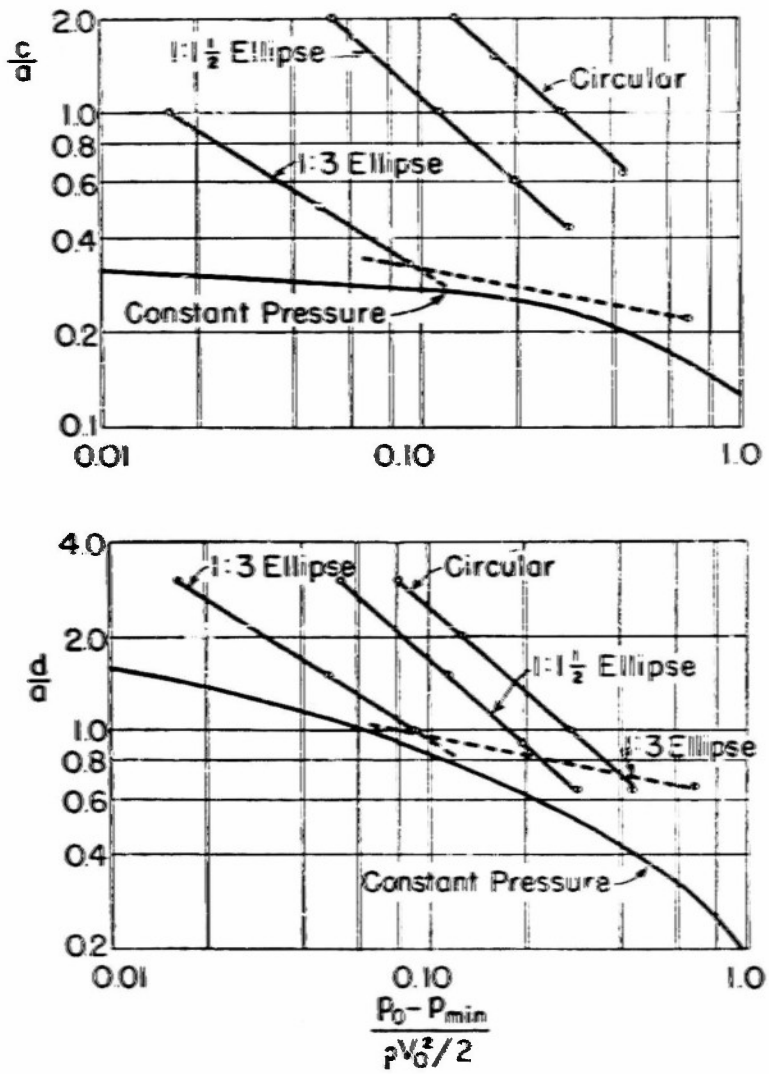

FIG. 5. COMPARISON OF DIMENSIONS OF VARIOUS TYPES OF TRANSITIONS.

The difference between axisymmetric and two-dimensional flow is such that a profile representing a compromise between the equal-curvature and equal-area profiles tested is necessary to give constant pressure in axisymmetric flow. Since a mathematical technique comparable to conformal transformations is not available, the general solution of the axisymmetric transition cannot be obtained. Specific cases, however, can be treated by relaxation techniques.

CONCLUSIONS

Equations have been obtained for the profiles of constant-pressure two-dimensional transitions and for the pressure distribution upstream and downstream from the transition. Perhaps the greatest advantage of this type of transition is that the minimum pressure can be specified. A comparison with other forms supports the supposition that the constant-pressure transition is the smallest possible for a given minimum pressure along the transition.

The limited experiments with flowing air indicated good correspondence between results of theory and of real fluid flows for high Reynolds numbers and for large contraction ratios. For lower Reynolds numbers and for smaller contraction ratios the correspondence was not as good because of the effects of viscosity.

DEFLECTION OF JETS
I. SYMMETRICALLY PLACED V-SHAPED OBSTACLE

by

T. T. Siao and P. G. Hubbard*

The deflection of a free jet by a solid boundary, which has long been utilized to develop power from flowing water, is well suited to free-streamline analysis because of the dominance of inertia and pressure intensity in the establishment of the flow pattern. The design of impulse machinery utilizing this momentum change could be facilitated greatly if the idealized geometry of the system under potential flow conditions were known, because such conditions represent asymptotic values which are approached as the effects of secondary variables are decreased. With such information available, refinements of design could be based upon a secure knowledge of the fundamentals, and many rules of thumb could be replaced with precise quantitative data in graphical or tabular form. Specifically, if the total angle through which the jet is deflected is determined for conditions of both partial and complete interception by the boundary, then the principle of impulse and momentum can be used to compute forces or other dynamic characteristics of the system.

This paper and the two which follow are devoted to a determination of the angles of deflection caused by certain idealized forms of solid boundaries placed either symmetrically or asymmetrically with respect to the axis of a two-dimensional jet. These patterns of flow correspond to those occurring as a bucket of an impulse machine passes through a circular jet. In this paper, the free-streamline method is used to find the angle through which a two-dimensional free jet will be deflected by a symmetrical V-shaped boundary placed on its axis.

As represented in Fig. 1a (the z-plane), a two-dimensional jet with velocity V_j and width $2a$ is deflected through an angle β by

*Research Associate and Research Engineer, respectively, Iowa Institute of Hydraulic Research, State University of Iowa, Iowa City.

the angular boundary of projected width $2b$. The sides of the boundary are inclined at an angle α relative to the original jet direction. In the hodograph plane (Fig. 1b), the bounding stream-

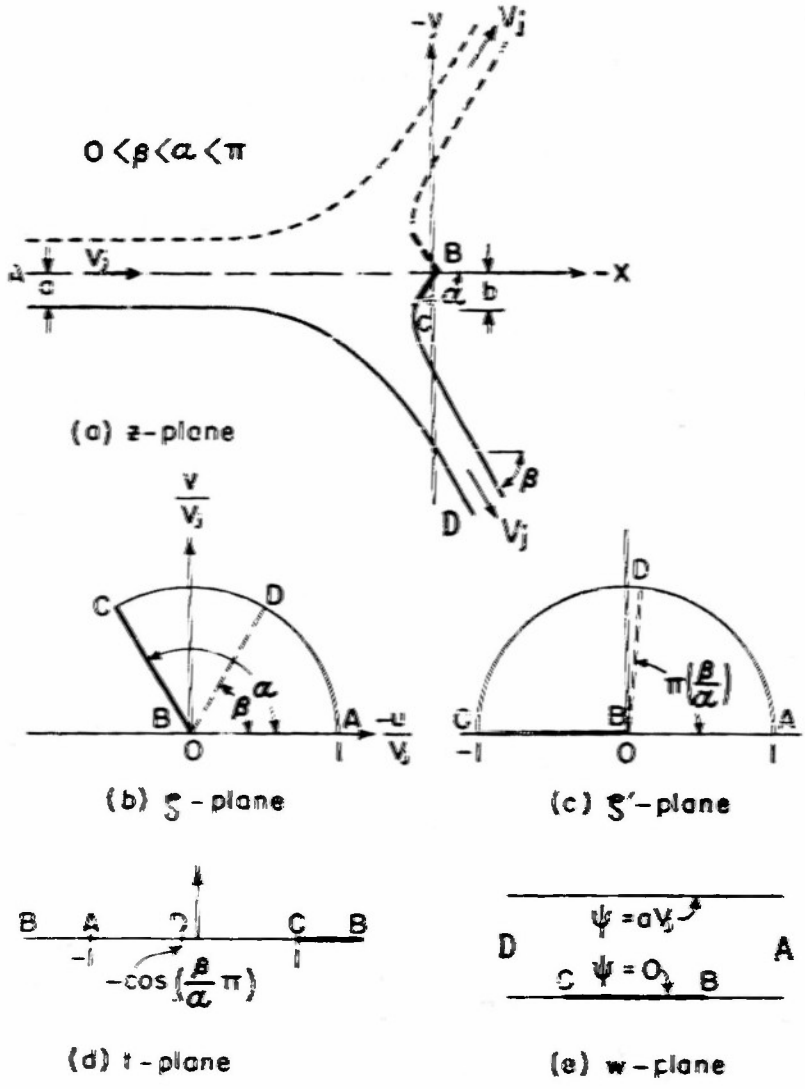

FIG. 1. TRANSFORMATION PLANES.

lines become a circular sector of angle α as can be shown from the definition relationship

$$\zeta = \frac{1}{V_j}\frac{dw}{dz} \tag{1}$$

in which w is the complex potential. (Details of this concept are

given in the first paper in this Bulletin.) This sector is expanded to a semicircle (Fig. 1c) by the transformation

$$\zeta' = \zeta^{\pi/\alpha} \tag{2}$$

and finally into the usual t-plane (Fig. 1d) by the transformation

$$t = -\frac{1}{2}\left(\zeta' + \frac{1}{\zeta'}\right) \tag{3}$$

In the t-plane, the flow pattern is simply that for a source with strength aV_j at A and a sink of equal strength at D for the flow occurring in the upper half of the plane. This latter requirement is satisfied if the strengths of the source and sink are doubled to provide an image pattern in the lower half (which actually represents the omitted half of the original system). Application of the usual equations for a source and a sink on the real axis then results in the potential function (Fig. 1e)

$$w = \frac{V_j a}{\pi}\left[\ln\left(t+\cos\frac{\pi\beta}{\alpha}\right) - \ln(t+1)\right] \tag{4}$$

From the purely analytical viewpoint, Eqs. (1), (2), (3), and (4) represent the solution to the problem, because proper manipulation of the variables will yield values of the velocity at any point in the physical plane. The explicit solution of these simultaneous algebraic and differential equations as they stand is quite involved, however, and the complexity of detail can be mitigated considerably by the introduction of an auxiliary variable τ, defined by

$$\tau = \zeta^{1/n} \tag{5}$$

and two positive integers m and n $(n < m)$ such that

$$\alpha = \frac{n}{m}\pi$$

Then, from Eq. (1)

$$dz = \frac{1}{V_j}\frac{dw}{\zeta} = \frac{1}{V_j \zeta}\frac{dw}{dt}\frac{dt}{d\zeta'}\frac{d\zeta'}{d\zeta}\frac{d\zeta}{d\tau}\,d\tau$$

and substitution of the appropriate derivatives from Eqs. (2-5) yields

$$dz = \frac{am}{\pi}\left[\frac{1}{\tau^m - e^{i\beta m/n}} + \frac{1}{\tau^m - e^{-i\beta m/n}} - \frac{2}{\tau^m - 1}\right]\tau^{m-n-1}\,d\tau$$

The resolving of this equation into partial fractions results in

$$dz = \frac{a}{\pi}\sum_{r=0}^{m-1}\left[\frac{e^{-i(2r\alpha-\beta)}}{\tau-e^{i(2r\alpha-\beta)/n}}+\frac{e^{-i(2r\alpha-\beta)}}{\tau-e^{i(2r\alpha-\beta)/n}}-\frac{2e^{-i2r\alpha}}{\tau-e^{i2r\alpha/n}}\right]d\tau \quad (6)$$

Integration of this equation between proper limits will give the coordinates in the z plane of any point corresponding to assigned values of α and β and of ζ. The differences in the coordinates of points B and C, for example, can be found by noting that, for the points B and C,

$$\zeta_B = 0 \quad , \quad \zeta_C = e^{i\alpha}$$

or

$$\tau_B = 0 \quad , \quad \tau_C = e^{i\alpha/n}$$

Thus, since B is the origin in the z-plane, integration of Eq. (6) between the limits of 0 and $e^{i\alpha/n}$ gives the coordinates of point C:

$$z_C = \frac{a}{\pi}\sum_{r=0}^{m-1}\Big\{e^{-i(2r\alpha+\beta)}\ln\left[1-e^{i(\alpha-2r\alpha-\beta)/n}\right] + e^{-i(2r\alpha-\beta)}\ln\left[1-e^{i(\alpha-2r\alpha+\beta)/n}\right] - 2e^{-i2r\alpha}\ln\left[1-e^{i(\alpha-2r\alpha)/n}\right]\Big\}$$

The imaginary part of this equation is the y-coordinate of point C, which is equal in absolute value to the distance denoted as b in the z-plane:

$$b=\frac{a}{\pi}\sum_{r=1}^{m-1}\sin\frac{2rn}{m}\pi\Big\{-\cos\beta\ln\left|\cos\frac{2r-1}{m}\pi-\cos\frac{\beta}{n}\right|+2\ln\sin\frac{2r-1}{2m}\pi\Big\} + \frac{a}{\pi}\sum_{r=0}^{m-1}\cos\frac{2rn}{m}\pi\sin\beta\ln\left|\frac{\sin\frac{1}{2}\left(\frac{2r-1}{m}\pi-\frac{\beta}{n}\right)}{\sin\frac{1}{2}\left(\frac{2r-1}{m}\pi+\frac{\beta}{n}\right)}\right|+a(1-\cos\beta) \quad (7)$$

Vertical bars in Eq. (7) indicate that absolute values are to be used.

Although analysts have already presented general solutions of jet intereceptions, and Cisotti [20] has completely solved the particular case of the normal plate, the method presented herein is considered more direct and the integrated solution is completed for the general case in Eq. (7). From this equation, values of b/a corresponding to assumed values of β have been computed for

various values of α. The results are plotted in Figs. 2 and 3, and several items of interest are immediately apparent. For example, a boundary with a projected width of twice the jet thickness cannot cause deflections greater than 90°, regardless of the angle at which it is placed. Similar conclusions could also be drawn for other relative width ratios. On the other hand, if the projected width of the boundary is four times the jet thickness, then the

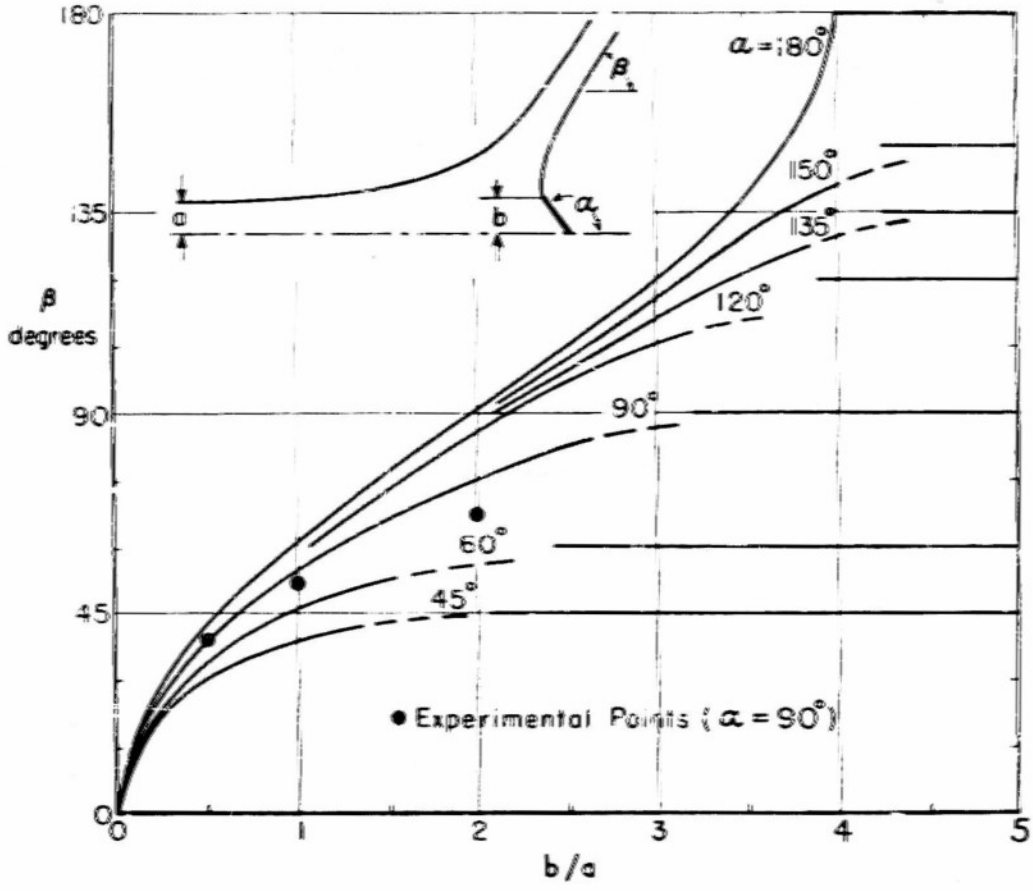

Fig. 2. Effect of Boundary Width on Jet Deflection.

jet deflection will be nearly complete ($\beta \to \alpha$) for all angles. This means, of course, that further widening of the deflector will increase the force exerted by only a small amount; the amount of possible increase is indicated by the 45-degree line corresponding to an infinitely wide deflector (Fig. 3).

In order to compare the results of this calculation with those observed for real axisymmetric flows, experiments were conducted in which a high-velocity circular jet of water was deflected by circular disks of various diameters (corresponding to $\alpha = \pi/2$).

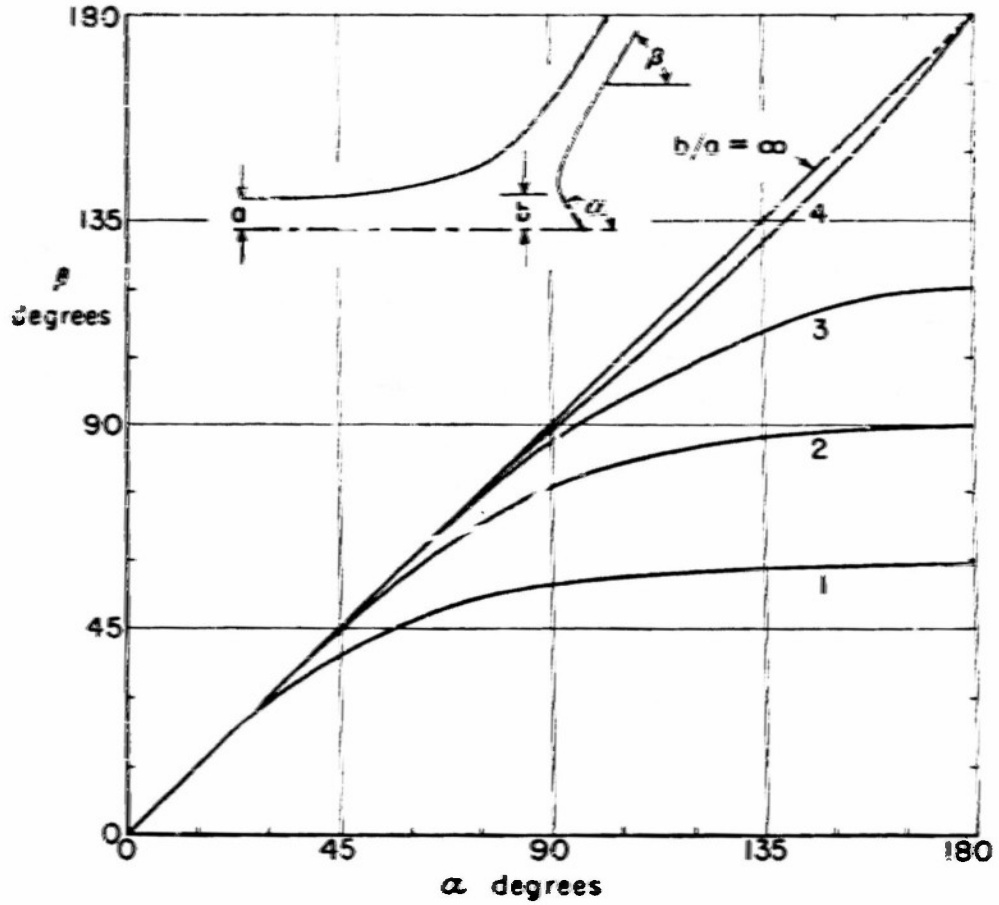

FIG. 3. EFFECT OF BOUNDARY ANGLE ON JET DEFLECTION.

Larger values of α would be used in an impulse machine, of course, but the normal disk is readily made and causes deflections which can be measured with an accuracy sufficient for comparison with computed values. The deflection β caused by each of three disks was measured from photographs taken with a camera mounted vertically above the disk to minimize errors due to the effect of gravity upon the stream.

Because the phenomenon under study is primarily one of momentum change, and because the area rather than the width enters linearly into momentum equations, it seems plausible that the area ratio should have more significance than the diameter ratio in comparing the axisymmetric experimental system with the two-dimensional analytic system. In the latter, of course, the areal and linear ratios are identical. In accordance with this concept, measured values of the deflection β have been included in Fig. 2,

the ratio of disk area to jet cross-sectional area having been used as the abscissa. From these points, it can be concluded that the deflector is less effective than computed values would indicate, and that there is an increasing discrepancy between computed and measured values as the area of the deflector increases. Comparative values of the momentum change are 96, 90, and 83 percent of the predictions for area ratios of 0.5, 1, and 2, respectively.

The correspondence between the measured values and the computed ones is illustrative of the degree of correlation between the idealized two-dimensional flows and comparable real flows of practical significance. As already indicated in the first paper of this series, the reasons for a lack of complete agreement can be determined by finding the ways in which the experimental system fails to meet the assumptions made in the mathematical analysis. In addition to the probable modifications of the flow pattern introduced by using an axisymmetric system rather than one of two dimensions only, it can be expected that viscous, gravitational, and possibly capillary effects may modify the flow to a measurable degree. Although the magnitude of the effects of these ignored parameters is difficult to determine, it can be shown that their influence in each case is in the proper direction to help account for the discrepancy actually found. For example, curvature of the path lines of the deflected sheet due to gravitational acceleration will decrease the apparent angle of deflection, and extraction of energy from the system by viscous friction at the deflector and at the large water-air interface will decelerate the flow and consequently decrease the angle of deflection. Capillary attraction at the solid-liquid-gas juncture where separation occurs should be small, but nonetheless will act to bend the flow in the direction measured, and surface tension in the deflected conical sheet will tend to resist the necessary increase in total area with distance as required by continuity principles applied to the axisymmetric case. This latter effect in particular would increase rapidly as the deflection angle becomes greater, and may account for the larger discrepancy found at larger angles.

In conclusion, the information made available and the close correlation between the results of free-streamline analysis and those of experiment are enough to warrant the recommendation of this method as a valuable supplement to existing methods employed in engineering design. Care must, of course, be exercised

in interpreting the results of computations of a two-dimensional flow pattern for a real system which is axisymmetric, as illustrated by the use of areal ratios rather than linear ratios in comparing the present results. For a system in which the flow pattern is determined primarily by inertia and pressure intensity, a knowledge of the true potential conditions is a valuable asset in assessing the effects of secondary variables and hence in judging what improvements are possible through reduction of secondary effects. In relation to the problem of Pelton-wheel design, it has been shown that the angle through which the jet is deflected can be substantially less than the angle of the bucket lip, approaching the latter value only if the projected area of the bucket is at least four times the jet area. This means that the bucket should be quite deep for practical angles of deflection, and that the bucket spacing may be affected. A combination of the results presented herein and those of the following two papers may prove valuable for further study of the Pelton-wheel design.

APPENDIX

In the preceding analysis the problem of a jet striking a wedge-shaped obstacle was solved by the method of conformal mapping. In that analysis the jet in consideration was free in the sense that it was not confined by any rigid boundary before it struck the object. However, in some applications of the preceding calculation, the approaching jet is not everywhere free but is rather confined in a pipe or channel. With the introduction of a straight boundary $\overline{BC}$, Fig. 4, the jet is no longer entirely free and the solution must be modified accordingly.

In Fig. 4, a confined jet of half width δ with an initial velocity V_0 proceeds towards the right, meets the barrier $\overline{AE}$ having an angle of inclination α to the direction of the approaching jet, and deflects through an angle β. The pattern obtained by revolving the figure about the axis AB corresponds to that of an axially symmetric flow through a cone valve [21]. The discharge coefficient is a function of the angle α, the opening s, and the dimension δ.

Application of Eqs. (1) and (2) transforms the flow in the z-plane into that within a half circle in the t-plane, with a source of strength $2dV_0$ at point B and a sink of equal strength at point D.

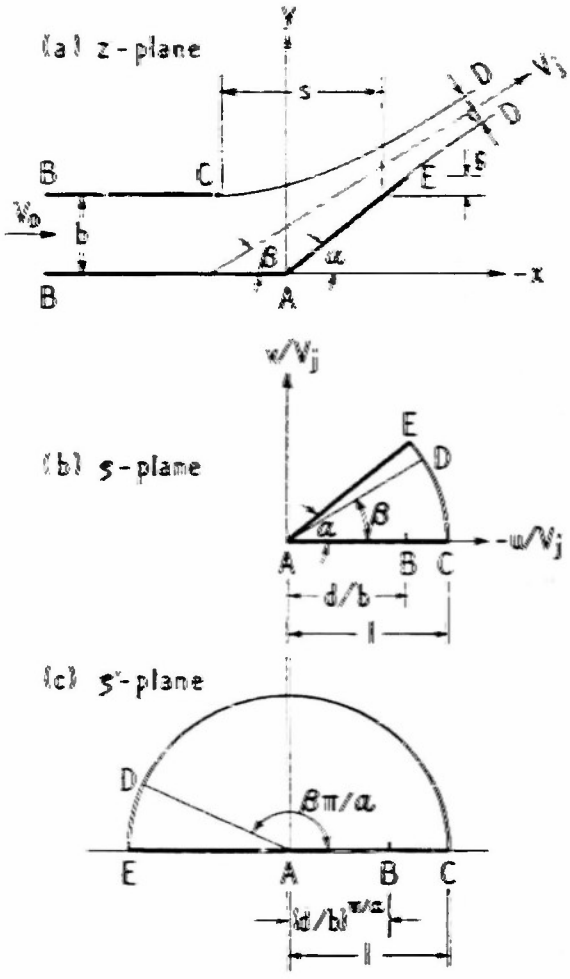

FIG. 4. TRANSFORMATION PLANES FOR CONFINED JET.

The complex potential for the source and sink and their images in the real axis and in the circle is

$$w = \frac{dV_j}{\pi} \ln \left[\frac{(\zeta' - e^{i\beta\pi/\alpha})(\zeta' - e^{-i\beta\pi/\alpha})}{(\zeta' - e^{i\pi/\alpha})(\zeta' - e^{-i\pi/\alpha})} \right] \tag{8}$$

in which $c = d/b$. By virtue of Eqs. (1), (2), and (8),

$$z = \frac{1}{V_j} \int \frac{1}{\zeta} dw = \frac{1}{V_j} \int \frac{1}{\zeta} \frac{dw}{d\zeta'} \frac{d\zeta'}{d\zeta} d\zeta$$

$$= \frac{d}{\alpha} \int \left[-\frac{1}{\zeta'^{\pi/\alpha} - e^{i\pi/\alpha}} - \frac{1}{\zeta'^{\pi/\alpha} - e^{-i\pi/\alpha}} \right.$$

$$\left. + \frac{1}{\zeta'^{\pi/\alpha} - e^{i\beta\pi/\alpha}} + \frac{1}{\zeta'^{\pi/\alpha} - e^{-i\beta\pi/\alpha}} \right] \zeta'^{\pi/\alpha - 1} d\zeta \tag{9}$$

If the substitutions

$$\alpha = \frac{n}{m}\pi \qquad , \qquad \tau = \zeta^{1/m}$$

are again made, m and n being any integers provided that $m > n$, then Eq. (9) reduces to

$$z = \frac{md}{\pi}\int\left[-\frac{1}{\tau^m - e^{\pi/\alpha}} - \frac{1}{\tau^m - e^{-\pi/\alpha}} + \frac{1}{\tau^m - e^{i\beta+\pi/\alpha}} + \frac{1}{\tau^m - e^{-i\beta+\pi/\alpha}}\right]\tau^{m-n-1}\,d\tau$$

$$= \frac{c}{\pi}\sum_{r=0}^{m-1}\int\left\{-\frac{e^{-1}e^{-i2r\alpha}}{\tau - e^{1/n}e^{i2r\alpha/n}} - \frac{ce^{-i2r\alpha}}{\tau - e^{-1/n}e^{i2r\alpha/n}} + \frac{e^{-i(2r\alpha+\beta)}}{\tau - e^{i(2r\alpha-\beta)/n}} + \frac{e^{-i(2r\alpha-\beta)}}{\tau - e^{i(2r\alpha-\beta)/n}}\right\}d\tau \qquad (10)$$

The integration of Eq. (10) carried out from $\tau = 0$ to $\tau = 1$ or to $\tau = e^{i\pi/n}$ gives values of z_C or z_E, respectively. The real part of z_C is equal to $b\cot\alpha - s$, and the imaginary part of z_E is equal to $\delta + b$. The final results are two equations expressing s and δ, respectively, as functions of c, α, and β.

For the special case of $\alpha = \pi/4$, m is 4 and n is 1; the final results are

$$-\frac{\pi\delta}{d} = (\cos\beta - \sin\beta)\ln\tan\frac{1}{2}\left(\frac{\pi}{4} + \beta\right) + (\cos\beta + \sin\beta)\ln\tan\frac{1}{2}\left(\frac{\pi}{4} - \beta\right) + \pi\cos\beta + \left(\frac{1}{c} + c\right)\tanh^{-1}\frac{2\sqrt{2}c}{1+c^2} + \left(\frac{1}{c} - c\right)\tan^{-1}\frac{2\sqrt{2}c}{1-c^2} \qquad (11)$$

and

$$\frac{\pi s}{d} = 2\cos\beta\ln\tan\frac{\beta}{2} + 2\sin\beta\ln\tan\frac{1}{2}\left(\frac{\pi}{2} - \beta\right) + \pi(\cos\beta + \sin\beta) + 2\left(\frac{1}{c} + c\right)\tanh^{-1}c + 2\left(\frac{1}{c} - c\right)\tan^{-1}c \qquad (12)$$

the values of the arctangent being taken between 0 and $\pi/2$. As $s \to \infty$, $c \to 1$, and from Eqs. (11) and (12), one obtains

$$-\frac{\pi\delta}{b} = (\cos\beta - \sin\beta)\ln\tan\frac{1}{2}\left(\frac{\pi}{4} + \beta\right) + (\cos\beta + \sin\beta)\ln\tan\frac{1}{2}\left(\frac{\pi}{4} - \beta\right) + \pi\cos\beta - 2\ln\tan\frac{\pi}{8} \qquad (13)$$

which corresponds with what has been derived before without the boundary BC. For another extreme case, $s \to 0$ and $c \to 0$, all dimensions must be expressed in ratios to s. Equations (11) and (12) reduce to

$$-\frac{\pi \delta/s}{d/s} = (\cos\beta - \sin\beta) \ln \tan \frac{1}{2}\left(\frac{\pi}{4} + \beta\right) + (\cos\beta + \sin\beta) \ln \tan \frac{1}{2}\left(\frac{\pi}{4} - \beta\right) + \pi \cos\beta + 4\sqrt{2} \quad (14)$$

and

$$\pi \frac{s}{d} = 2\cos\beta \ln \tan \frac{\beta}{2} + 2\sin\beta \ln \tan \frac{1}{2}\left(\frac{\pi}{2} - \beta\right) + \pi(\cos\beta + \sin\beta) + 4 \quad (15)$$

The above analysis constitutes the preliminary investigation leading to the discussion by one of the writers of the paper "Characteristics of Fixed Dispersion Cone Valves" [21]. In that discussion the evaluation of the discharge coefficient for cone valves by an analysis of the corresponding plane flow and a comparison of the calculated results with the test ones are given in detail; in the following, only its essential points are given.

The discharge coefficient is obtained by dividing the discharge by the product of the flow area and $\sqrt{2gH}$. Put in equation form,

$$C = \frac{Q}{A\sqrt{2gH}} \quad (16)$$

in which A is the area of efflux and H is the total head. For the two-dimensional flow the corresponding discharge coefficient is d/s.

A logical approach to the adaptation of these results for plane flow to the determination of the discharge coefficient for the corresponding three-dimensional flow is to assume that corresponding ratios between the initial and the final area of the jet are the same in each case (as they were found to be for the orifice [15]). That is,

$$C = \frac{d}{s} = \frac{\text{the ultimate value of } w(2\pi x)}{s(2\pi BB')} \quad (17)$$

in which w is the thickness of the three-dimensional jet at a certain point and x the distance from that point to the x-axis.

The values of C and β have been plotted in Fig. 5 against s/D,

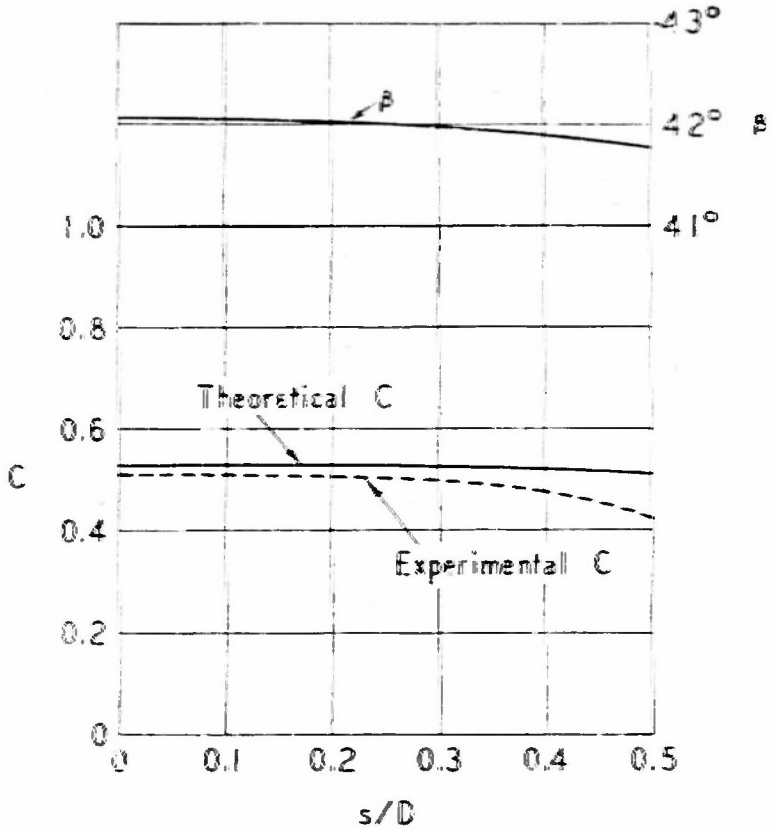

FIG. 5. VARIATIONS OF DEFLECTION ANGLE AND COEFFICIENT OF CONTRACTION WITH OPENING.

(which is equal to $s/2b$). A mean curve has been drawn for the test results obtained by Messrs. Elder and Dougherty. The correspondence between the test results and those of the analysis is fairly good for values of s/D up to about 0.3.

The present problem has been treated by Greenhill [22, pp. 26-29] who gave the essential steps of the solution. However, the solution presented in the foregoing is much simpler and has been carried to the numerical stage.

DEFLECTION OF JETS

II. SYMMETRICALLY PLACED [_]-SHAPED OBSTACLE

by

TURGUT SARPKAYA*

As an alternative to the approximation of a bucket on a Pelton wheel in the preceding paper, a channel-shaped deflector can be considered. As pointed out by Greenhill [21], a shape for which the irrotational flow pattern can be computed is a symmetrical plate with two right-angled bends which would be tangent to the usual bucket as shown in Fig. 1. This approximation in conjunction with that presented in the preceding paper should provide an insight into the relative importance of the bucket geometry in a determination of the angle through which the jet is deflected.

As indicated in Fig. 2a, a jet of width $2d$ impinges on a [_]-shaped boundary with web height $2a$ and flange width b, and each half of the jet is deflected through an angle $\pi - \beta$. From the Bernoulli

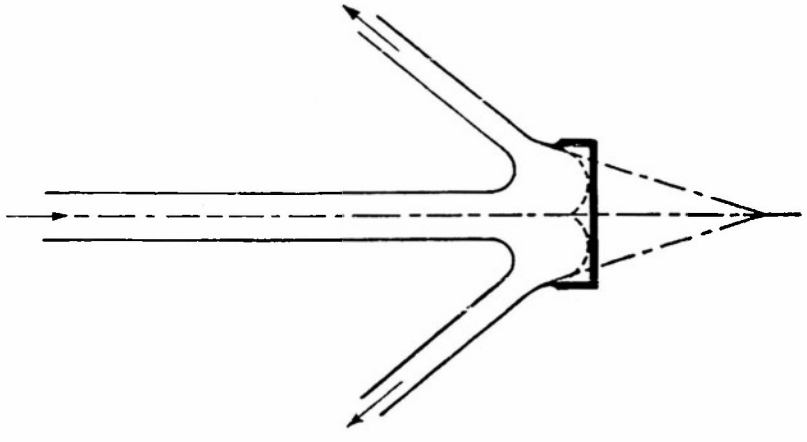

FIG. 1. COMPARISON OF JET DEFLECTION BY VARIOUS OBSTACLES.

equation the velocity of approach V_j of the incident jet is seen to be the same as the asymptotic velocity of the deflected jets, and from the equation of continuity the thickness of each of the de-

*Research Assistant, Iowa Institute of Hydraulic Research, State University of Iowa, Iowa City.

flected jets is seen to be precisely d. The total force exerted by the fluid on the solid boundary can be computed from the momentum principle once the angle of inclination β of the deflected jets, which depends only on a/d and b/d, is known. Thus, definition of the relationship

$$\beta = f(a/d \ , \ b/d) \tag{1}$$

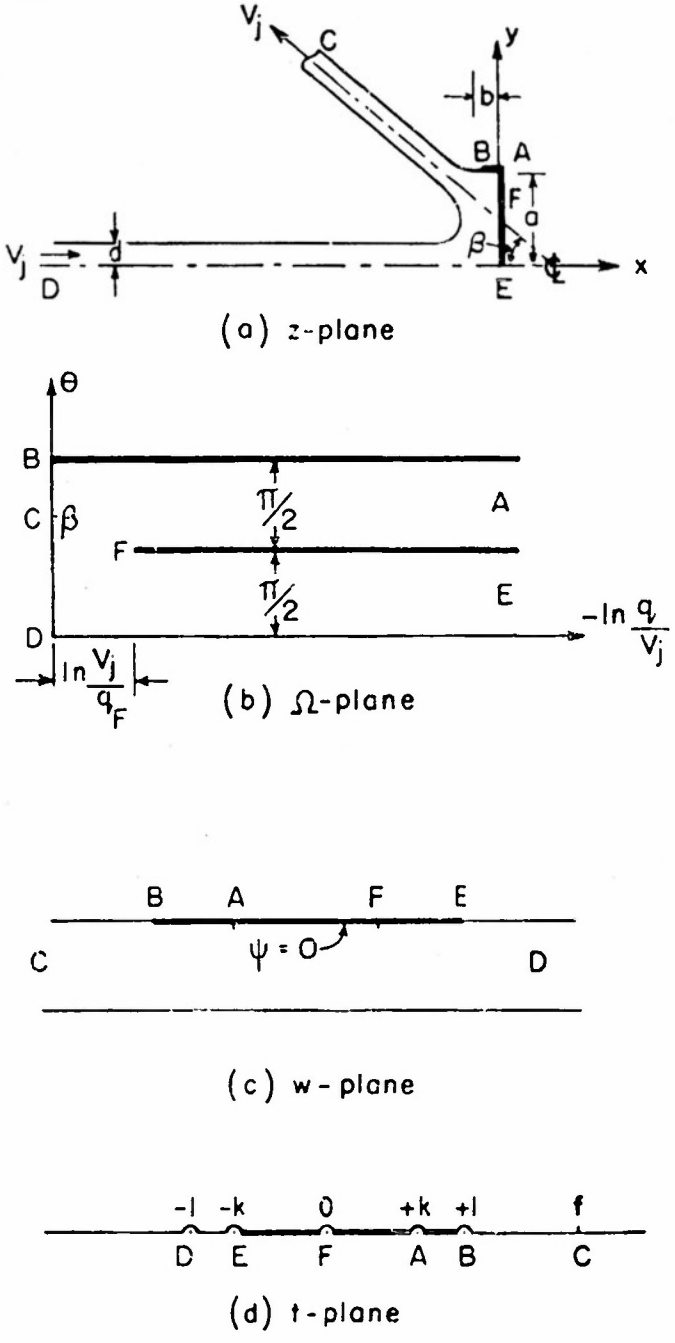

FIG. 2. TRANSFORMATION PLANES.

is the main objective of the present investigation. For convenience, the point of maximum velocity along the solid boundary between E and A is designated by the letter F.

If, as in the other papers contained in this Bulletin, z and w are used for the complex variable and the complex potential, then the variable ζ defined as dw/dz is given by

$$\zeta = -u + iv = -q e^{-i\theta} \tag{2}$$

in which u and v are the velocity components in the x- and y-directions, q is the magnitude of the velocity vector, and θ is its angle of inclination.

If the variable Ω,

$$\Omega = \ln\left(-\frac{V_j}{\zeta}\right) = -\ln\frac{q}{V_j} + i\,\theta \tag{3}$$

is introduced, the flow region in the physical plane (Fig. 2a) can be mapped onto a corresponding region in the Ω-plane, as indicated in Fig. 2b. This latter region is in turn mapped onto the upper half of the auxiliary t-plane.

As indicated in Fig. 2d, the values -1, 0, and 1 are assigned to the points D, F, and B in the t-plane. The values of t for E, A and C can be denoted by $-k$, k, and f, respectively, those for E and A being of equal magnitude and opposite signs due to symmetry. The desired mapping between Ω and t is then achieved by the use of the Schwarz-Christoffel transformation

$$\Omega = \int \frac{A\,t\,dt}{(t^2-k^2)\sqrt{t^2-1}} = \frac{A}{\sqrt{1-k^2}} \ln\frac{\sqrt{1-k^2}+\sqrt{1-t^2}}{\sqrt{t^2-k^2}} \tag{4}$$

in which A is found to be $\sqrt{1-k^2}$ by substituting into the equation the coordinates of the point B in the two planes, positive values having been assigned to the radicals between D and E.

Because of the singularities at $t = \pm k$ and at $t = \pm 1$, the function Ω given by Eq. (4) must be evaluated with reference to a path (as shown in Fig. 2d) which has semi-circular indentations at each of these points, real values being assigned to Ω along DE. As can be readily verified, Eq. (4) transforms the upper half of the t-plane into the region in the Ω-plane shown in Fig. 2b. In particular, it will be noticed that

$$i\beta = \ln \frac{\sqrt{1-k^2}+\sqrt{1-f^2}}{\sqrt{f^2-k^2}} = i \sin^{-1} \frac{\sqrt{f^2-1}}{\sqrt{f^2-k^2}}$$

so that

$$\beta = \sin^{-1} \frac{\sqrt{f^2-1}}{\sqrt{f^2-k^2}} \tag{5}$$

In the limiting case, $k = 0$, and the last formula gives $f = \sec \beta$.

The complex potential w can be expressed in terms of t by the method of sources and sinks:

$$w = \frac{V_2 d}{\pi} \left[\ln (t-f) - \ln (t+1) \right]$$

From this relationship and from the definition of ζ,

$$z = \frac{V_2 d}{\pi} \int \frac{1}{\zeta} \left[\frac{1}{t-f} - \frac{1}{t+1} \right] dt$$

so that, from Eqs. (3) and (4),

$$z_A - z_B = ia = \frac{i d}{\pi} I_1 \tag{6}$$

in which

$$I_1 = -\int_{-k}^{+k} \frac{\sqrt{1-t^2}+\sqrt{1-k^2}}{\sqrt{k^2-t^2}} \left[\frac{1}{t-f} - \frac{1}{t+1} \right] dt$$

Similarly,

$$z_A - z_B = b = \frac{d}{\pi} I_2 \tag{7}$$

in which

$$I_2 = \int_{-1}^{-k} \frac{\sqrt{1-k^2}+\sqrt{1-t^2}}{\sqrt{t^2-k^2}} \left[\frac{1}{t+1} + \frac{1}{f-t} \right] dt$$

The integrals I_1 and I_2 are evaluated in the Appendix. If various values are assigned for f and k, the corresponding values of β, a, and b can be calculated from Eqs. (5), (6), and (7). The results are presented graphically in Fig. 3.

A solution for the limiting case of an infinitely deep bucket can be obtained without recourse to complicated analysis. In this instance, the velocity is zero at the bottom of the cup and the

pressure is correspondingly $\rho V_j^2/2$. The momentum equation (with reference to Fig. 2a) for the x-direction is thus

$$2\rho V_j^2 d + 2\rho V_j^2 d \cos\beta = \rho V_j^2 a$$

or

$$a = 2d(1 + \cos\beta) \tag{8}$$

which is a limiting form of Eq. (6). It follows that the maximum value of a/d is 4 for this special case, as was also noted in the preceding paper in which this limit was considered as the 180° V-shaped deflector. Another limiting case is that of the simple flat plate which is approached as b tends toward zero.

In experiments conducted by Mr. DeHaven, observations were made of the angle through which jets were deflected by variously proportioned cups of cylindrical shape. These are compared with the values calculated for two-dimensional flows in Fig. 3. In spite of the fact that the experiments were performed for flow with axial symmetry whereas the theoretical calculations are based on two-dimensional flow, the agreement between the results obtained

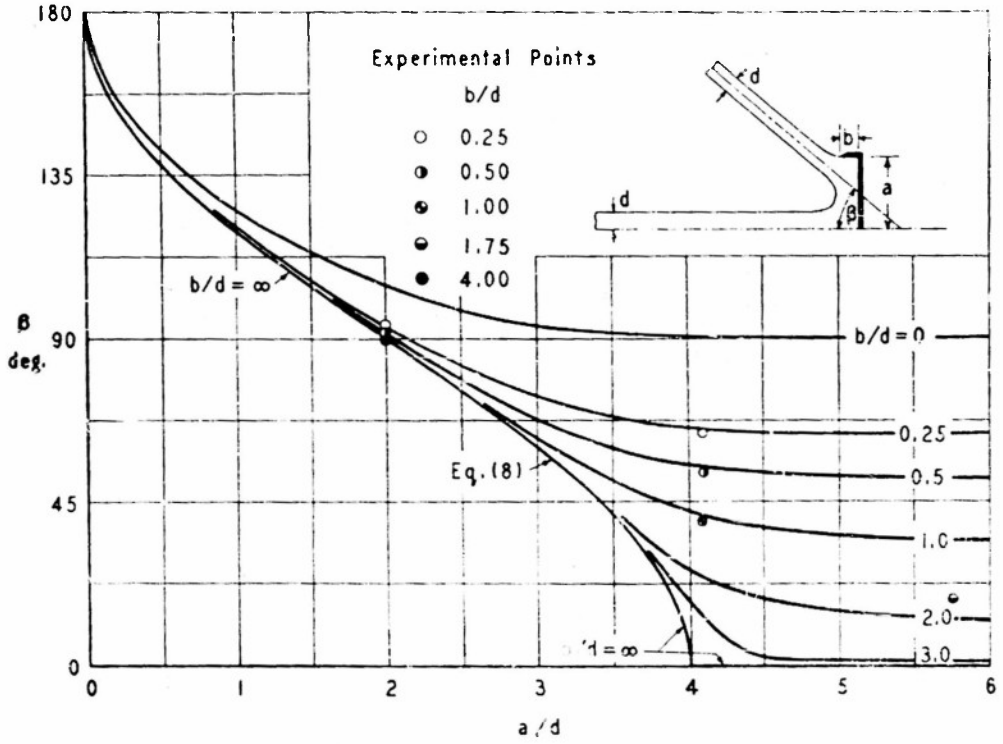

FIG. 3. ANGLE OF DEFLECTION AS A FUNCTION OF THE DIMENSIONS OF THE OBSTACLE.

from experiments and those calculated from theory, equal area ratios being assumed, is excellent.

Professor H. T. Muhly of the mathematics department suggested methods for the evaluation of the integrals encountered. Mr. T. T. Siao familiarized the author with the problem, and the Editors assisted extensively in the preparation of the manuscript.

APPENDIX

The integral I_1 can be decomposed into five component integrals:

$$I_1 = \sqrt{1-k^2}\int_{-k}^{+k} \frac{dt}{(t+1)\sqrt{k^2-t^2}} \quad \ldots\ldots A$$

$$+\sqrt{1-k^2}\int_{-k}^{+k} \frac{dt}{(f-t)\sqrt{k^2-t^2}} \quad \ldots\ldots B$$

$$+(1-f^2)\int_{-k}^{+k} \frac{t\,dt}{(f^2-t^2)\sqrt{(k^2-t^2)(1-t^2)}} \quad \ldots C$$

$$+(1+f)\int_{-k}^{+k} \frac{dt}{\sqrt{(k^2-t^2)(1-t^2)}} \quad \ldots\ldots D$$

$$+f(1-f^2)\int_{-k}^{+k} \frac{dt}{(f^2-t^2)\sqrt{(k^2-t^2)(1-t^2)}} \quad \ldots E$$

in which A, B, and C are elementary integrals and can be taken from tables, and

$$D = 2(1+f)\int_0^1 \frac{du}{\sqrt{(1-u^2)(1-k^2u^2)}} = 2(1+f)K(k)$$

K, being the complete elliptic integral of the first kind, is given in tables of elliptic functions for various values of k. Thus only the integral E remains to be evaluated. If the following substitutions are made,

$$t = k\tau\,, \qquad \left(\frac{k}{f}\right)^2 = \mu\,, \qquad k^2 = m$$

one has

$$E = 2\,\frac{1-f^2}{f}\,F(1,\mu,m) \tag{9}$$

in which

$$F(x,\mu,m) = \int_0^x \frac{d\tau}{(1-\mu\tau^2)\sqrt{(1-\tau^2)(1-m\tau^2)}}$$

is an elliptic integral of the third kind. Unfortunately, this integral has not been tabulated, so that one is obliged to express it in terms of other functions.

If one writes $\tau = \mathrm{sn}\,(u,k)$ and $x = \mathrm{sn}\,(y,k)$, in which $\mathrm{sn}\,(u,k)$ is an elliptic function of Jacobi defined implicitly by

$$u = \int_0^{sn\,(u,k)} \frac{ds}{\sqrt{(1-s^2)(1-k^2s^2)}}$$

then the integral $F\,(x,\mu,m)$ becomes

$$F_1(y,\mu,m) = \int_0^v \frac{\mathrm{cn}\,u\,\mathrm{dn}\,u\,du}{(1-\mu\,\mathrm{sn}^2\,u)\sqrt{\mathrm{cn}^2\,u\,\mathrm{dn}^2\,u}} = \int_0^v \frac{du}{1-\mu\,\mathrm{sn}^2\,u}$$

$$= y + \mu\int_0^v \frac{\mathrm{sn}^2\,u\,du}{1-\mu\,\mathrm{sn}^2\,u} \tag{10}$$

in which $\mathrm{sn}\,u$ is written for $\mathrm{sn}\,(u,k)$. If a new quantity c is defined by

$$\mu = m\,\mathrm{sn}^2\,(c,k) = m\,\mathrm{sn}^2\,c$$

so that

$$c = \mathrm{sn}^{-1}\left(\frac{1}{f},\ k\right)$$

then

$$\int_0^v \frac{\mathrm{sn}^2\,u\,du}{1-\mu\,\mathrm{sn}^2\,u} = \frac{1}{m\,\mathrm{sn}\,c\,\mathrm{cn}\,c\,\mathrm{dn}\,c}\,\Pi(y,c) \tag{11}$$

with

$$\Pi(y\ c) = \int_0^v \frac{m\,\mathrm{sn}\,c\,\mathrm{cn}\,c\,\mathrm{dn}\,c\,\mathrm{sn}^2\,u}{1-m\,\mathrm{sn}^2\,c\,\mathrm{sn}^2\,u}\,du$$

$$= y\,Z(c,k) + \frac{1}{2}\ln\left[\frac{\Theta(y-c)}{\Theta(y+c)}\right]$$

in which $Z(c, k)$ and Θ are respectively the Zeta-function and the Theta-function of Jacobi. Since the function $\Theta(y, c)$ is an even function with the periods K and K' given by

$$K = \int_0^1 \frac{dt}{\sqrt{(1-t^2)(1-k^2t^2)}} = \mathrm{sn}^{-1}(1, k), \qquad K' = \mathrm{sn}^{-1}(1, \sqrt{1-k^2})$$

one has

$$\Theta(K-c) = \Theta(K+c)$$

so that

$$\Pi(K, c) = KZ(c, k) + \frac{1}{2}\ln\frac{\Theta(K-c)}{\Theta(K+c)} = KZ(c, k) \qquad (12)$$

Thus, from Eqs. (9) to (12), one obtains, on putting $y = K$,

$$E = 2\frac{1-f^2}{f}K\left[1 + \frac{\mu Z(c, k)}{m\ \mathrm{sn}\ c\ \mathrm{cn}\ c\ \mathrm{dn}\ c}\right]$$

Since

$$\mathrm{sn}^2(c, k) + \mathrm{cn}^2(c, k) = 1 \quad , \quad \mathrm{dn}^2(c, k) + m\,\mathrm{sn}^2(c, k) = 1$$

$$\mathrm{cn}(c, k) = \frac{\sqrt{f^2-1}}{f} \quad , \quad \mathrm{sn}(c, k) = \frac{1}{f}$$

$$\mathrm{dn}(c, k) = \frac{\sqrt{f^2-k^2}}{f} \quad , \quad \mathrm{sc}(c, k) = \frac{1}{\sqrt{f^2-1}}$$

one has, finally,

$$E = 2\frac{1-f^2}{f}K\left[1 + \frac{fZ(c, k)}{\sqrt{f^2-1}\sqrt{f^2-k^2}}\right]$$

and the evaluation of I_1 is completed:

$$I_1 = \pi \pm \pi\frac{\sqrt{1-k^2}}{\sqrt{f^2-k^2}} + 2(1+f)K + 2\frac{1-f^2}{f}K\left[1 + \frac{fZ(c, k)}{\sqrt{f^2-1}\sqrt{f^2-k^2}}\right]$$

in which the plus or minus sign is used depending on whether f is greater than 1 or less than -1. Similarly, the evaluation of the integral I_2, for both negative and positive values of the parameter f, can be accomplished. The results are:

$$I_2 = -\ln\left(1-\sqrt{1-k^2}\right) - 2\tanh^{-1}\sqrt{\frac{1-k}{1+k}}$$

$$\pm 2\frac{\sqrt{1-k^2}}{\sqrt{f^2-k^2}}\tanh^{-1}\frac{\sqrt{(f+k)(1-k)}}{\sqrt{(f-k)(1+k)}} + (1+f)K'$$

$$-fK'\left\{1+\frac{\sqrt{f^2-1}}{f\sqrt{f^2-k^2}}\left[Z(c,k)+\frac{\pi c}{2KK'}\right]-\frac{1}{f^2}\right\}-\frac{\pi}{2}\frac{\sqrt{f^2-1}}{\sqrt{f^2-k^2}}$$

with the same convention for signs.

For numerical calculations, use has been made of the tables of Jacobian elliptic functions by Milne-Thomson [23]. An account of the theory of Jacobian elliptic functions can be found in [24].

DEFLECTION OF JETS
III. UNSYMMETRICALLY PLACED SEMI-INFINITE PLATE

by

SIMON INCE* and CLARK DEHAVEN*

Deflection of a jet by a plate is a problem in hydraulic engineering for which a theoretical solution can be obtained only in very particular instances. The method of calculation of the force exerted by a jet impinging perpendicularly on a plate of infinite dimensions is shown in most textbooks of fluid mechanics. Mathematical treatment of similar problems for somewhat more complex circumstances, however, is not possible, and acceptable approximations must be

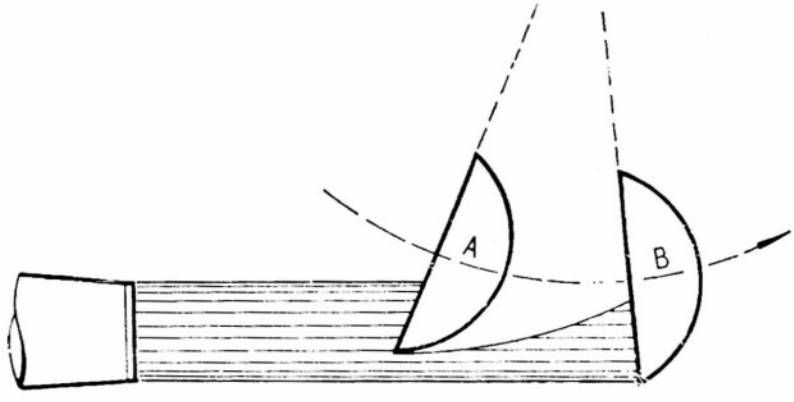

FIG. 1. CUSTOMARY CONCEPTION OF JET DIVISION BY PELTON-WHEEL BUCKETS.

made unless experimental data are available. Thus, in the conventional design of a Pelton wheel it is expedient, for want of more accurate information, to assume that the portion of the jet deflected by the bucket is in simple proportion to the penetration of the bucket, and that the remainder of the jet continues in a straight line, as shown in Fig. 1.

A theoretical analysis of the two-dimensional counterpart of this problem should shed some light on the general problem and possibly be of some value to turbine designers. Although there is

*Research Associates, Iowa Institute of Hydraulic Research, State University of Iowa, Iowa City.

no mathematical justification for the application of these theoretical results to actual three-dimensional flows, this approach seemed promising in view of the fortuitous correspondence between results of theory for two-dimensional flows and those of experiments for three-dimensional flows which has been noted previously in the cases of contraction coefficients for cone valves, orifices, and manifolds.

The conditions of flow in a Pelton wheel indicated in Fig. 1 can be approximated if the flow is considered to be two-dimensional and the buckets to be simple flat plates. Considered in this analysis is the general case of a two-dimensional jet impinging on a semi-infinite flat plate, as indicated schematically in Fig. 2a in which

a is the thickness of the initial jet,
d is the perpendicular penetration of the plate into the jet,
γ is the angle which the plate makes with the horizontal,
b is the thickness of the guided portion of the deflected jet,
β is the ultimate angle, measured counter-clockwise, which the free portion of the jet makes with the horizonal, and
V_∞ is the velocity of the jet at infinity.

The ratio of the division of flow b/a and the ultimate angle of the jet β are to be defined in terms of the penetration d at various inclinations of the plate.

From the energy principle it is seen that the velocities at A, B, and E (each of which is at an infinite distance from D) must all be equal for irrotational flow. From application of the momentum equation in the direction parallel to the plate, the relationship

$$b + (a - b)\cos(\beta + \gamma) - a\cos\gamma = 0 \qquad (1)$$

is obtained.

From Fig. 2a a geometrical relationship between b, d, and β can be found:

$$d = a - \oint dy = a - (a-b)\cos\beta + k \qquad (2)$$

in which the contour integration is performed along DEA, and

$$k = \int_{DE} dy + \int_{EA} dy$$

As shown in the following calculation, it is convenient to calculate

d indirectly from Eq. (2) rather than to assign values to it. For a given angle γ, a division of flow is assumed and the angle β is

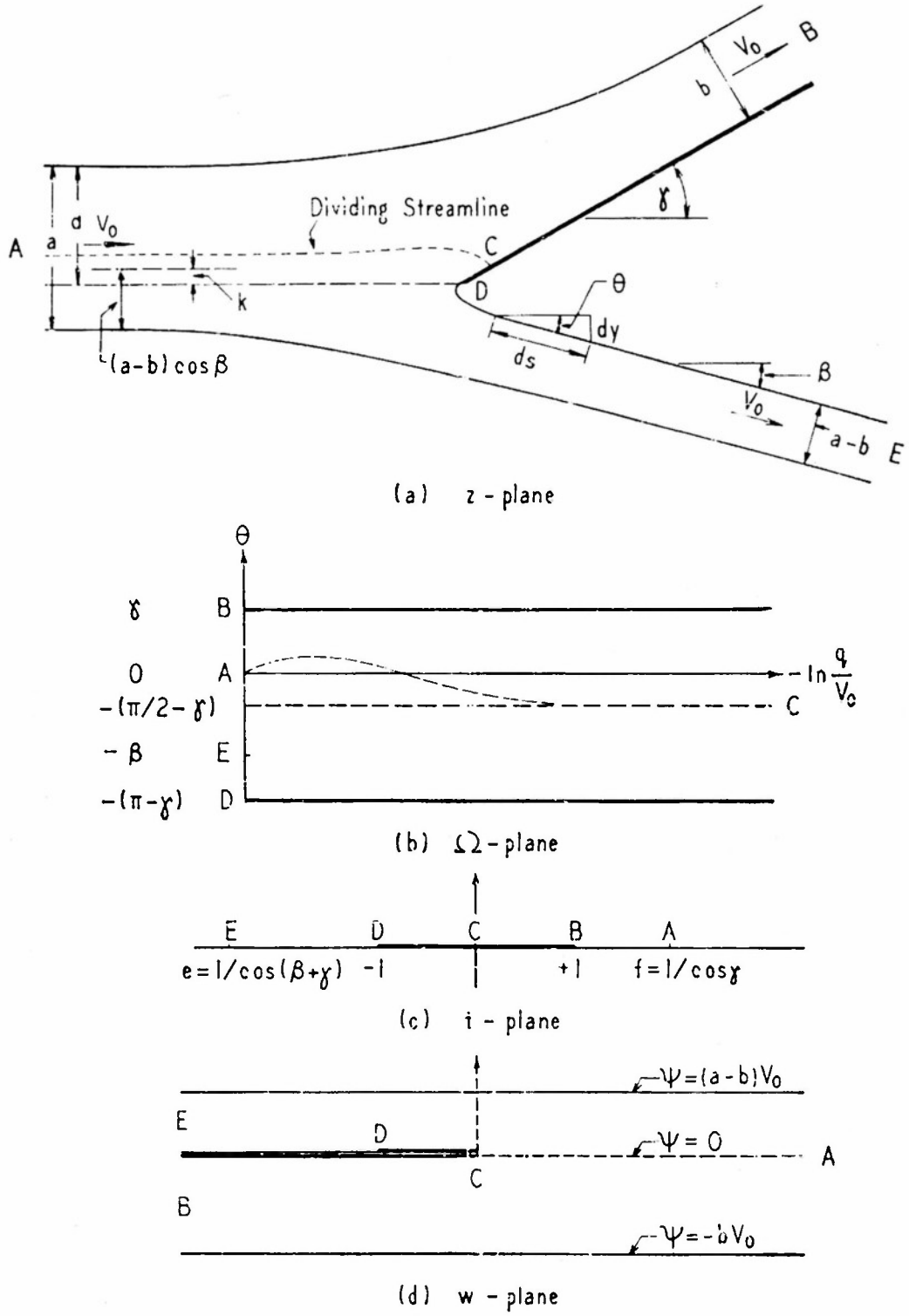

FIG. 2. CONFORMAL MAPPING PLANES.

determined from the momentum relationship. If the value of k for this particular case can be calculated in terms of a, b, γ, and β, then Eq. (2) yields the corresponding value of d. Thus the problem is reduced to the determination of k.

From Fig. 2a, $dy = \sin\theta\, ds$, θ being the variable angle of inclination of the jet and s being measured along the contour. Then, along DE and EA, $V_0 ds = -d\phi$, in which ϕ is the velocity potential, and one has

$$k = -\int_{DE} \frac{\sin\theta}{V_0}\, d\phi - \int_{EA} \frac{\sin\theta}{V_0}\, d\phi \tag{3}$$

Geometrically, k is the distance between the horizontal line through D and the horizontal asymptote to the streamline EA after EA is shifted a distance $a-b$ in a direction normal to the inclined asymptotes of DE and EA. In region A this shifting results in the lower streamline being moved upwards a vertical distance equal to $(a-b)\cos\beta$. The integration depends upon the expression of ϕ in terms of θ, and this is accomplished by the use of conformal transformations.

The logarithmic hodograph of the flow pattern, denoted as the Ω-plane and shown in Fig. 2b, is obtained from the relationship,

$$\Omega = -\ln\frac{q}{V_0} + i\theta \tag{4}$$

in which q is the magnitude of the variable velocity vector and θ the angle that it makes with the horizontal. The interior of the semi-infinite strip of the Ω-plane is mapped onto the upper half of the t-plane (Fig. 2c) by means of a Schwarz-Christoffel transformation, the connecting relationship being

$$\Omega = -i\cos^{-1}\frac{1}{t} + i\gamma \tag{5}$$

The w-plane is shown in Fig. 2d. The transformation equation between the w-plane and the t-plane is obtained directly from the complex potentials for sources and sinks, point A being considered as a source of strength $2aV_0$ and points B and E as sinks of strengths $2bV_0$ and $2(a-b)V_0$, respectively:

$$w = \frac{V_0}{\pi}\left\{b\ln(t-1) + (a-b)\ln(t-e) - a\ln(t-f)\right\} + M \tag{6}$$

in which M is a complex constant. After introducing the relation-

ship $dw = d\phi + id\psi$ and noting that along a streamline $d\psi = 0$, and hence $dw = d\phi$, one can write the contour integral as

$$k = -\oint \frac{\sin\theta}{V_0} dw$$

If dw is replaced by the corresponding value from Eq. (6), the expression for k becomes

$$k = -\frac{1}{\pi}\int_{-1}^{1} \sin\theta \left\{\frac{b}{t-1} + \frac{a-b}{t-e} - \frac{a}{t-f}\right\} dt \qquad (7)$$

Also, since $q = V_0$ along the free streamlines, Ω is simply $i\theta$ for all points on DE and $D'E'$ from Eq. (4).

Introduction of this value into Eq. (5) and solution for t yield the relationship,

$$t = \sec(\gamma - \theta) \qquad (8)$$

which is valid for all points on the free streamlines. If now the values of t in Eq. (7) are expressed in terms of θ from Eq. (8), the limits of integration for θ ($\gamma - \pi$ and 0) taken from the Ω-plane, and the resulting expression integrated, the value obtained is

$$k = \frac{1}{\pi}\left\{b\sin\gamma \ln\frac{2b}{a(1+\cos\gamma)-2b} + a\sin\gamma\cos\gamma \ln\frac{2[a(1+\cos\gamma)-2b]}{b(1+\cos\gamma)}\right.$$
$$\left. -(a-b)\cos\gamma\sin(\beta+\gamma)\ln\left(\cos\gamma + \cot\frac{\beta}{2}\sin\gamma\right)\right\} \qquad (9)$$

in which

$$\sin(\beta+\gamma) = \frac{\sqrt{a(1-\cos\gamma)[a(1+\cos\gamma)-2b]}}{a-b}$$

Discussion of Results

Equation (9) has been evaluated for various divisions of flow and for plate angles equal to 30°, 45°, 60°, 90°, 120°, and 150°. The corresponding values of plate penetration and deflection angle are presented in graphical form, with b/a and β plotted against d/a (Figs. 3 and 4).

It was noted with considerable concern at first that for very small values of b/a, the penetrations of the plate d/a were small negative values. Since a thorough check of the calculations revealed no errors, further confirmation was sought by comparison with

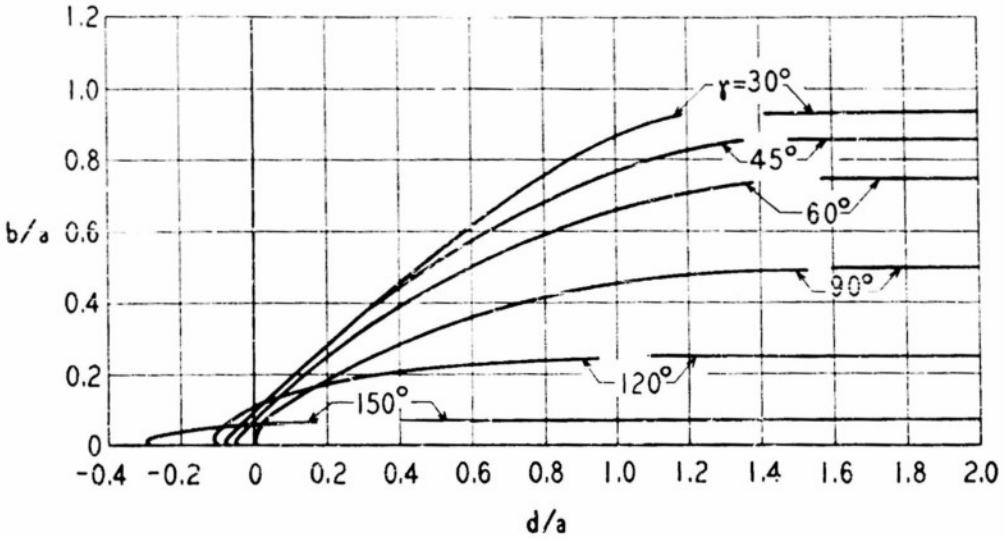

FIG. 3. FLOW DIVISION AS A FUNCTION OF PLATE PENETRATION.

the results of Love [25], who treated the general case of the oblique impact of a jet upon a finite lamina. Following the method indicated by Love, the equations of the free streamlines were calculated for the case of $\gamma = \pi/2$, and the value of the penetration

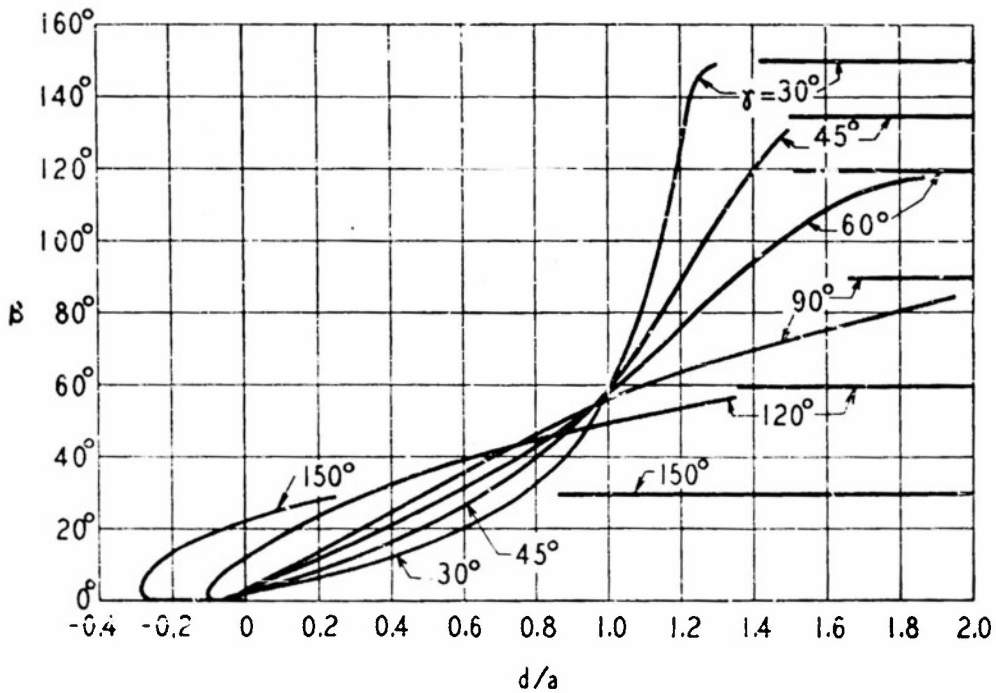

FIG. 4. DEFLECTION ANGLE AS A FUNCTION OF PLATE PENETRATION.

computed. Identical negative penetrations were obtained from this independent check.

The physical anomaly of a finite division of flow by a plate lying outside the path of the jet assumes an immediate significance, however, if it is considered that the negative of the complex function w also satisfies the Laplacian equations. The physical interpretation of the negative w function corresponds to a reversal of

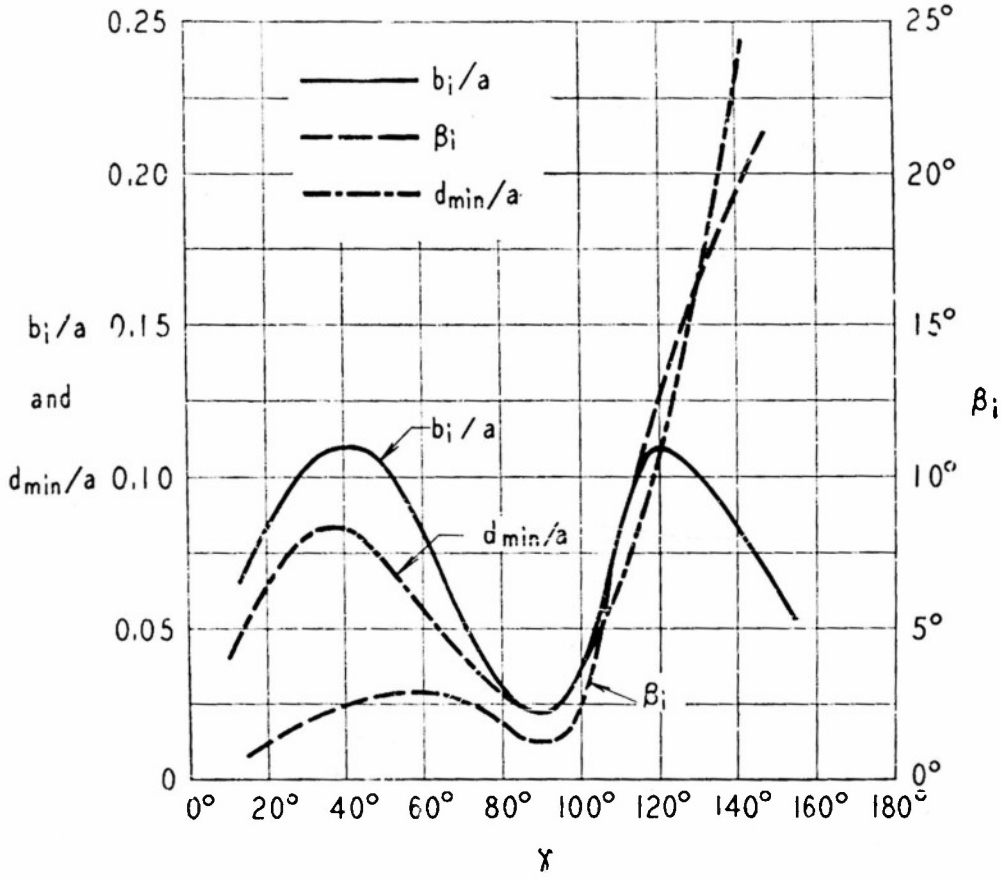

FIG. 5. VARIATIONS OF b_i/a, β_i AND d_{min}/a WITH γ

the direction of flow. The resulting physical phenomenon in the case under consideration is then that of a free jet joining a guided jet near the end of the guiding plate, the combined flow continuing as a horizontal free jet. As can be seen from the several graphs, there is a limit to the so-called "negative penetration" determined by the requirement of the continuity and momentum relationships. The variation of d_{min} with γ is shown in Fig. 5.

The behavior of b/a and β in the region of negative penetration

is indicated in Fig. 6, which is drawn to a greatly enlarged scale. It can be clearly seen that as b/a increases from 0 to 0.02, d/a decreases first to its minimum value of -0.00243, and then increases to 0. From this point on, the analysis can be considered to represent the problem posed at the outset of this investigation. The physical explanation of this phenomenon is that an infinitesimal penetration ϵ causes a finite initial angle of deflection β_i and a

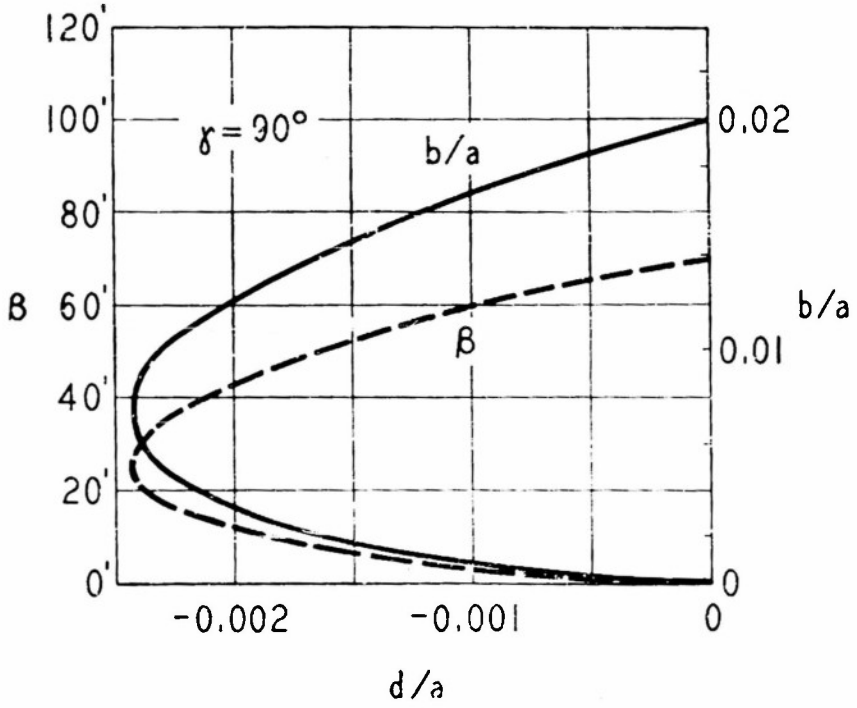

FIG. 6. DEFLECTION ANGLE AND DIVISION OF FLOW FOR NEGATIVE PENETRATIONS ($\gamma = 90°$).

finite initial division of flow b_i/a. Figure 5 contains a plot of values of β_i and b_i/a as functions of the plate angle γ.

In the region of positive penetration there is, for a given γ, an asymptotic limit to the deflection angle β and the corresponding division of flow as the penetration is increased to infinity (Figs. 3 and 4), these limits having been determined for the various plate angles by means of the momentum relationship.

An attempt was made to verify experimentally the results obtained by theoretical analysis. A jet of water with a nominal diameter of 1.5 inches was penetrated by a plate, and the division of flow and angle of deflection were measured. Since the momentum relationship is the determining factor, the area ratio of the divided

jet was substituted for the b/a ratio of the two-dimensional case.

Although the experimental results verify the general trends of the analysis (Figs. 3 and 4), there are, nevertheless, discrepancies of as much as 50% from the predicted values. Part of these can be attributed to the crudities of the experimental arrangement, although it is recognized that a significant source of error may well lie in the inherent differences between two- and three-dimensional flows. Thus the fortuitous correspondence between two-dimensional theory and its three-dimensional counterpart which has been encountered in other investigations does not materialize in this instance.

However, it is obvious from analysis and experiment that neither of the two common assumptions mentioned in the introduction to this paper is valid. That is, in considering the flow into Pelton-wheel buckets, (a) the division of flow b/a is not in simple proportion to the penetration d/a, and (b) the unguided portion of the jet does not continue in the same straight line, but is deflected through a considerable angle. Thus, as shown in Fig. 1, the portion of the jet not caught by bucket A is generally assumed to be caught by bucket B, whereas, due to the deflection of the jet, it may actually miss the wheel entirely.

In view of the uncertainties of the applicability of the simplified theory to the complex shapes of Pelton-wheel buckets, and in view of the lack of complete experimental confirmation throughout the full range of the analysis, no positive recommendations can be made until more representative analyses and complete experiments are available. Nevertheless, despite the lack of general quantitative results for circular jets striking buckets on Pelton wheels, the manner in which a jet is divided and deflected has been indicated qualitatively as a guide for design.

MANIFOLD EFFLUX

by

ARTHUR TOCH* and ROBERT W. MOORMAN**

INTRODUCTION

In navigation locks and turbine scroll cases, water is often supplied to the lock chamber or to the turbine through a manifold system. The resultant flows have been the subject of many model studies for the solving of specific design problems or the obtaining of general information regarding the flow phenomena involved. Also, mathematical treatment of manifold flow was made by McNown and Hsu [12] in which certain phases of the flow were evaluated.

A manifold can be represented in its simplest form by an opening in the wall of a straight conduit. The lateral can thus be eliminated or a lip of any length can be added. This representation corresponds to some forms of constructions actually used [26] and was the basis for the analysis by McNown and Hsu. A different type of manifold is also used, in which the conduit changes in cross section either in steps at each lateral or continuously over most of its length [27]. The analysis in this paper pertains to this stepped form for the particular case of the infinitely long lateral. Correlation of the results of the mathematical treatment with experimentally obtained values for these manifolds is also discussed.

MATHEMATICAL ANALYSIS

A view of the two-dimensional manifold is shown in the z-plane of Fig. 1. Flow with velocity V_B occurs in the conduit of width b. Part of the flow enters the infinitely long lateral through an opening of width a and attains, after contraction of the flow section to

*Research Associate, Iowa Institute of Hydraulic Research, State University of Iowa, Iowa City.

**Now Associate Professor of Mechanics and Hydraulics, Clemson Agricultural College, Clemson, South Carolina.

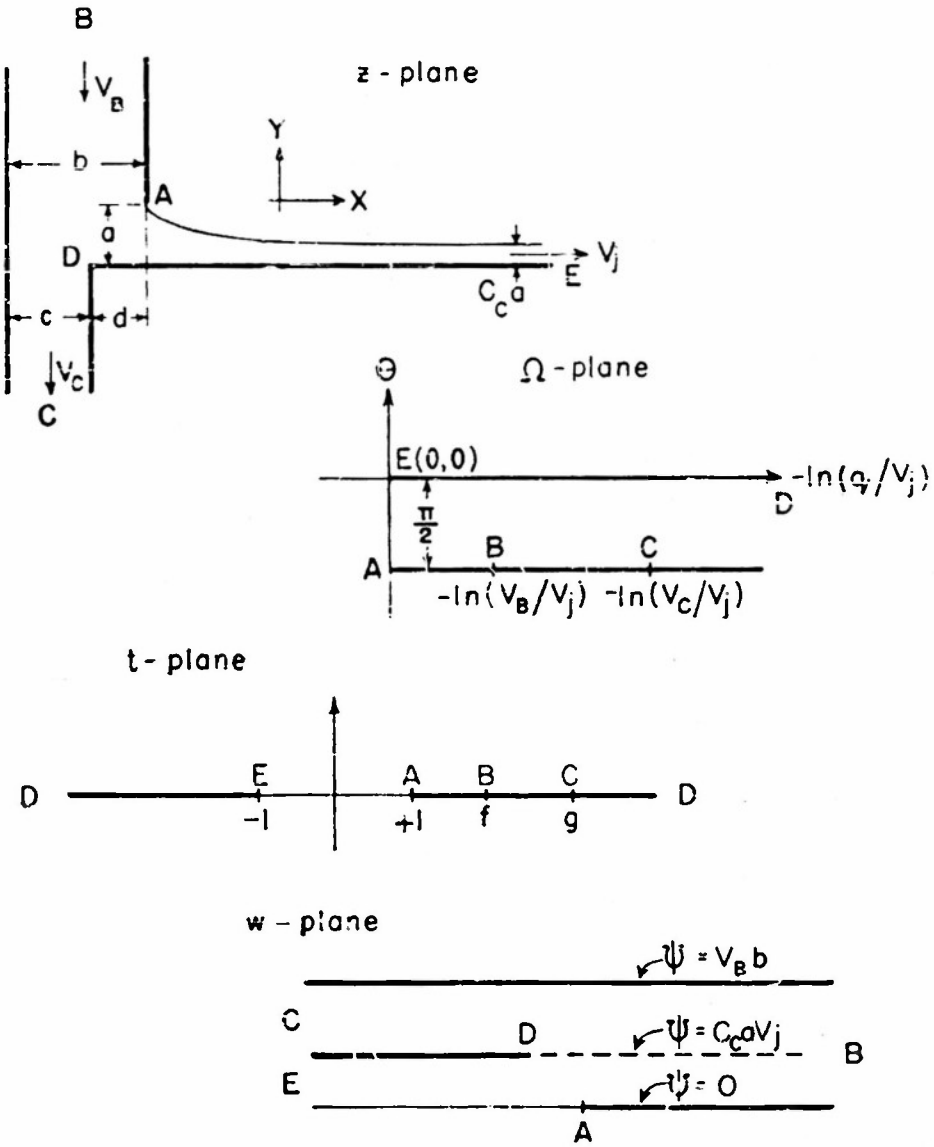

FIG. 1. TRANSFORMATION PLANES.

$C_c a$ at infinity, a velocity V_j. The remainder of the flow continues in a conduit of width c and attains an ultimate velocity V_C. The difference between the initial and final widths of the conduit is denoted by d.

Evidently, the evaluation of a coefficient of contraction C_c and of a velocity ratio V_C/V_B as functions of the boundary geometry is the primary objective of the present investigation. The boundary geometry is expressed by the ratios a/b and d/b, so that the desired functions are

$$C_c = f_1 (a/b, d/b)$$

and

$$V_C/V_B = f_2 (a/b, d/b)$$

In order to determine these relationships, the complex function w must be defined as a function of z; the manifold shown in the z-plane is thus related to a simpler shape, the infinite rectangle of the w-plane. Two intermediate planes are needed to obtain this indirect mathematical relationship. The first of these intermediate planes is the logarithmic hodograph or Ω-plane of Fig. 1. The velocities along the boundaries of the z-plane are plotted through use of the definition equation

$$\Omega = -\ln \frac{1}{V_j} \frac{dw}{dz} = -\ln \frac{q}{V_j} + i\theta \tag{1}$$

In this equation q/V_j is the ratio of any velocity in the z-plane to the final jet velocity in that plane, and θ is the angle formed between the velocity vector and the x-axis.

In the other intermediate plane, the t-plane, the boundary of the flow is prescribed to coincide with the real axis. Thus the Schwarz-Christoffel transformation can be used, which here takes the form

$$\Omega = M \cosh^{-1} t + N$$

The semi-infinite rectangle of the Ω-plane now becomes the upper half of the t-plane. Three points can be arbitrarily located in this plane. Points A and E are accordingly placed on the horizontal axis at equal distances from the origin and are assigned the values of $+1$ and -1, respectively, and D is placed at infinity, as shown. The values of M and N in the transform can be evaluated by substituting simultaneous values of Ω and t for the points A, E, and D, in successive steps. Then,

$$\Omega = \frac{1}{2} \operatorname{cosh}^{-1} t - i\frac{\pi}{2} \tag{2}$$

The final step in relating the manifold in the z-plane to the infinite rectangle in the w-plane is also accomplished by means of the Schwarz-Christoffel transformation,

$$w = \phi + i\psi = M' \int \frac{dt}{(t-f)(t-g)(t-1)} + N'$$

After integration of this equation, the constant M' can be evaluated by equating the differences in the imaginary parts of the two sides of the equation for points A, B, and C. The additive constant N' is similarly determined from the difference in the real parts of the quantities at D and E. Introduction of the values of M' and N' in the integrated transformation yields

$$w = -\frac{b}{\pi}\frac{V_B}{V_j}\ln(t-f) + \frac{c}{\pi}\frac{V_C}{V_j}\ln(t-g) + \frac{C_c a}{\pi}\ln(t+1) + C_c a \quad (3)$$

The distances f and g shown on the t-plane and occurring in Eq. (3) can be expressed as functions of the velocity ratios. To this end, the expression for Ω of Eq. (1) is introduced in Eq. (2) and the resulting equation evaluated at point B, so that

$$f = \frac{1}{2}\left(\frac{V_B^2}{V_j^2} + \frac{V_j^2}{V_B^2}\right)$$

and at point C, so that

$$g = \frac{1}{2}\left(\frac{V_C^2}{V_j^2} + \frac{V_j^2}{V_C^2}\right)$$

Once the transformations are completed, the opening a can be related to the lateral efflux by integration across the flow:

$$a = \int_{AE} dy + C_c a$$

The integral can be evaluated after proper substitutions have been made. If s is defined as the distance along the free streamline measured from A in the z-plane, the relationship,

$$dy = \sin\theta\, ds$$

is obtained.

Because $\psi = 0$ along the streamline AE, as indicated in the w-plane (Fig. 1), $\partial w/\partial s = \partial\phi/\partial s$ between A and E. By definition, $\partial\phi/\partial s = -V_j$; and dy can now be expressed as

$$dy = -\frac{\sin\theta}{V_j}\, d\phi$$

From Eqs. (1) and (2),

$$\sin\theta = \sqrt{\frac{1}{2}(t+1)}$$

along AE. If the last two expressions are substituted into the equation for a,

$$a - C_c a = \oint_{AE} \frac{1}{V_j} \sqrt{\frac{1}{2}(t+1)}\, d\phi$$

in which $d\phi$ can be expressed in terms of t by Eq. (3). The resulting integral can be written as

$$a - C_c a = \frac{b}{\pi\sqrt{2}} \frac{V_B}{V_j} \int_{+i}^{-1} \frac{\sqrt{t+1}}{t-m}\, dt - \frac{c}{\pi\sqrt{2}} \frac{V_C}{V_j} \int_{+1}^{-1} \frac{\sqrt{t+1}}{t-n}\, dt$$

$$- \frac{C_c a}{\pi\sqrt{2}} \int_{+1}^{-1} \frac{\sqrt{t+1}}{t+1}\, dt \qquad (4)$$

in which the limits are evident from examination of the t-plane.

The evaluation of this integral is comparatively straight-forward, and this form was chosen for that reason. Other substitutions than the above, or use of a hodograph (ζ-plane), result in integrals of more complex form. That the resultant equations will be identical to the one obtained from Eq. (4) is obvious. The tediousness of these other integrations makes mention of them worthwhile, however, because integration for another flow model may well be easiest in another plane.

The three integrals in Eq. (4) were evaluated separately, and values of f and g were substituted to give the final expression,

$$a - C_c a = \frac{2}{\pi}\left[b\left(\frac{V_B^2}{V_j^2} + 1\right)\tanh^{-1}\frac{V_B}{V_j} - c\left(\frac{V_C^2}{V_j^2} + 1\right)\tanh^{-1}\frac{V_C}{V_j}\right] \qquad (5)$$

The premise of continuity, implicit in the above discussion, can be stated as

$$V_B b - V_C(b-d) - V_j C_c a = 0 \qquad (6)$$

Although Eqs. (5) and (6) determine the general flow field, another equation is necessary to impose a particular stagnation condition which is physically applicable. The reference velocities and the dimensions of the boundary should satisfy a requirement that the horizontal and the vertical velocity components on the dividing streamline will vanish simultaneously at D. On the Ω-plane (Fig. 2), if BFD corresponds to the dividing streamline, v will vanish before u if the stagnation point D is approached. Similarly, if BGD corresponds to the dividing streamline, u will vanish be-

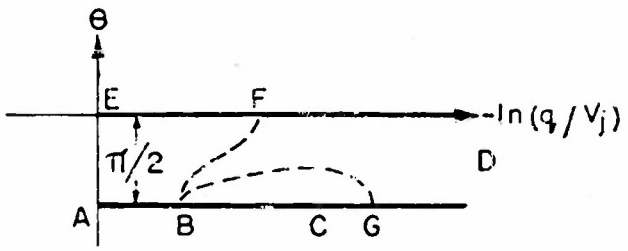

FIG. 2. DIVIDING STREAMLINE IN LOGARITHMIC HODOGRAPH.

fore v. The condition that u and v should vanish simultaneously, therefore requires F, or G, to approach D.

The line BFD, or BGD, is a streamline issuing from the source B, the Ω-plane being viewed as another physical plane for a fictitious flow with F, or G, as the stagnation point. Thus at F, or G, $dw/d\Omega = 0$, and since

$$\frac{dw}{dt} = \frac{dw}{d\Omega}\frac{d\Omega}{dt} = \frac{dw}{dt}\frac{1}{2\sqrt{t^2-1}}$$

in which t is different from ± 1,

$$\frac{dw}{dt} = 0$$

The last equation characterizes the point F, or G. If t approaches zero, after substitution of w from Eq. (3) in the last equation, a condition is obtained which is equivalent to the requirement that F, or G, should coincide with D. This condition equation is

$$V_j C_c\, a = V_C\, b\, g - V_C\, d\, g - V_B\, b\, f \tag{7}$$

In [12], this point was overlooked; it was called to the attention of the authors of that paper by A. Craya of Grenoble, France. As a consequence, their results include the cases for which F, or G, is not at point D. A statement of this fact was made in [28] but no analytical result was presented.

Equations (5), (6), and (7) can now be arranged to obtain

$$\frac{a}{b} = \frac{V_C}{V_j}g - \frac{V_B}{V_j}f - \frac{d}{b}\left[\frac{V_C}{V_j}g - F\left(\frac{V_C}{V_j}\right)\right] + \left[F\left(\frac{V_B}{V_j}\right) - F\left(\frac{V_C}{V_j}\right)\right] \tag{8}$$

$$\frac{d}{b} = 1 - \left[\frac{V_B}{V_C}\left(\frac{V_B}{V_j}+\frac{V_j}{V_B}\right)^2 \Big/ \left(\frac{V_C}{V_j}+\frac{V_j}{V_C}\right)^2\right] \tag{9}$$

and

$$C_c = \frac{\frac{V_B}{V_j} - \frac{V_C}{V_j}\left(1 - \frac{d}{b}\right)}{a/b} \tag{10}$$

in which

$$F\left(\frac{V}{V_j}\right) = \frac{2}{\pi}\left[1 + \left(\frac{V}{V_j}\right)^2\right] \tanh^{-1}\left(\frac{V}{V_j}\right)$$

The values of the velocities V_B and V_C relative to V_j in these equations must also satisfy Eqs. (5) to (7). The two functional relationships mentioned earlier as the primary objective of the analysis are now replaced by three parametric equations.

Numerical calculation of Eqs. (8) to (10) yields the graphs shown in Figs. 3 and 4, or comparable ones if the coordinate axes

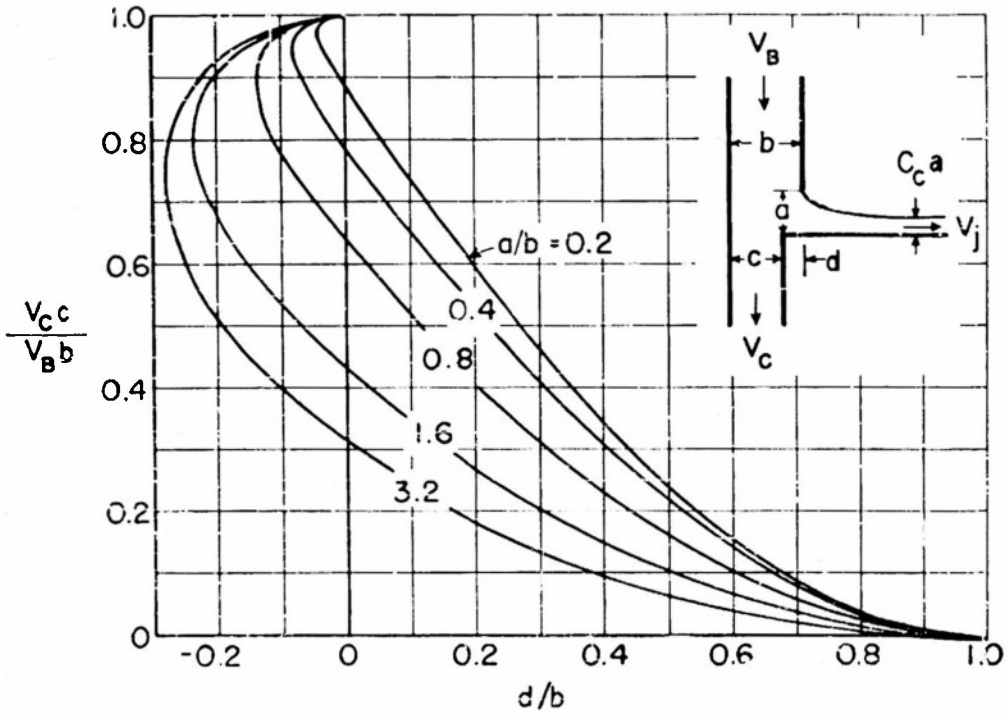

FIG. 3. EFFLUX CHARACTERISTICS OF THE INFINITE LATERAL.

are chosen differently. The graphs indicate more clearly, of course, than do the equations, the flow conditions possible under the assumptions made. In Fig. 3 the ratio d/b is shown to be negative as well as positive. The negative sign denotes merely that the

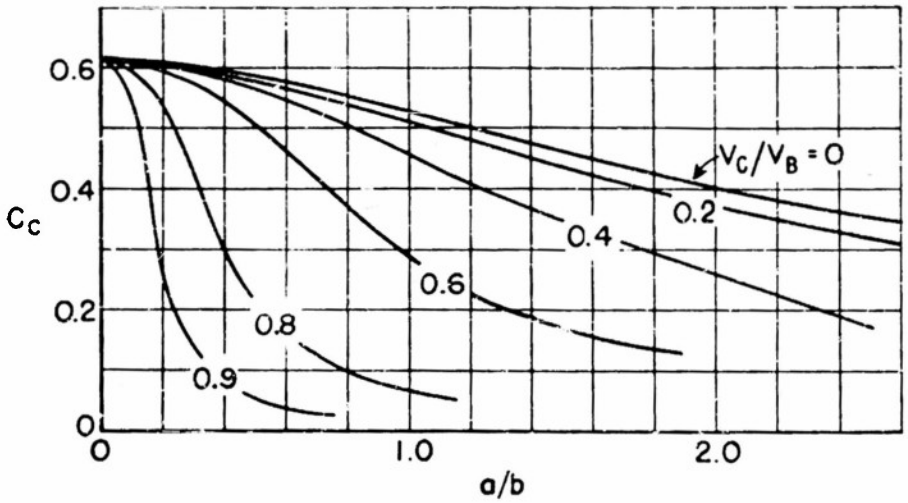

FIG. 4. CONTRACTION COEFFICIENT FOR THE INFINITE LATERAL.

downstream conduit width c is greater than b. As a/b approaches zero, a limiting value of $\pi/(\pi + 2)$ for C_c is obtained, as shown on Fig. 4. The ratio of the conduit velocities is the other parameter determining C_c, larger values indicating less efflux through the lateral and, therefore, greater contraction.

EXPERIMENTAL VERIFICATION

As mentioned in the introduction, an analysis [12] was previously made of the manifold with an opening in the side of the conduit. Comparison of the results of that investigation with those of experiments with an orifice in one side of a lock conduit [26] is made in Fig. 5. The curve, in each of the two graphs, is the mathematical relationship and the points plotted are the experimental values. The agreement between the trends of experiment and hydrodynamic theory is remarkable, because the calculations are based on two-dimensional flow, whereas the actual flow was definitely three-dimensional.

Although this agreement is heartening, it must be viewed as fortuitous. The attempt at verifying experimentally the model set forth in this paper was completely unsuccessful. In the laboratory model used to verify the theory, the coefficient of contraction could not be measured, because a reverse eddy formed at the jet surface. The attempt was made, therefore, to correlate the

velocity ratios with the geometry of the dividing flow. This proved to be impossible, not so much because the dividing stream surface was hard to determine by means of the dye injection used, but because the flow pattern showed considerable divergence from two-dimensional conditions.

Agreement between calculation and experiment depends on the physical applicability of the assumptions made in the mathematical derivation. Values shown in Fig. 5 were obtained with free efflux from a sharp-edged port. The water jet was thus surrounded by air, a condition which comes close to satisfying the assumption of a velocity discontinuity involved in the free-streamline theory. The

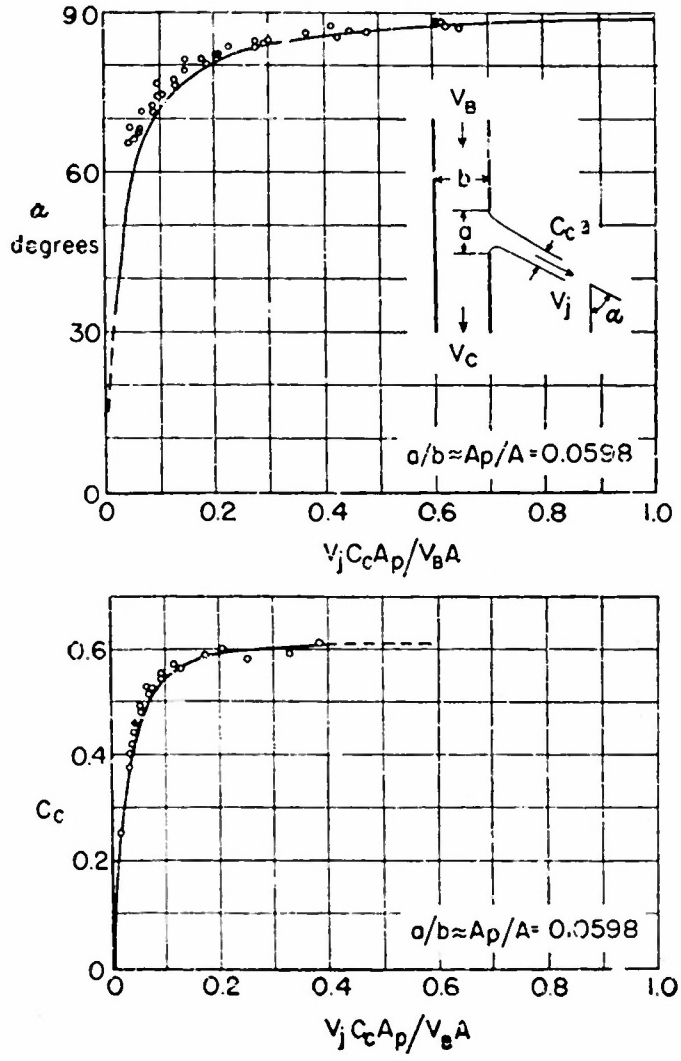

FIG. 5. EFFLUX CHARACTERISTICS OF AN ORIFICE IN A CONDUIT.

infinite lateral was, of necessity, a branch conduit, and a reverse eddy occurred in the lateral beside the jet. Although some experimental evidence [12] exists which indicates that for high-velocity submerged jets the eddy does not invalidate the assumption, for the low-velocity jet in this experiment the assumption was hardly approximated. The tendency of the lateral to draw a disproportionate share of low-velocity fluid from the conduit, as observed by Barton and Escobar [28], may also be of importance in this case.

CONCLUSION

Of the several possible types of manifold efflux, two were considered in this paper. For these, the use of the free-streamline theory of hydrodynamics provided a good approximation to efflux from a port in the conduit but failed to describe the flow into a lateral.

The disagreement between the limited experimental results and the relationships obtained from the mathematical analysis presented in this paper results from the lack of applicability to this real flow of the assumptions implicit in the theory. That such lack need not nullify the use of the theory, however, is indicated by the results obtained for port efflux. Although other conditions of real flow may also be compatible with the free-streamline theory, the range of applicability cannot be determined from the limited evidence at hand.

HEAD LOSSES IN MITER BENDS

by

HARRY H. AMBROSE*

The sudden deflection of flow produced by a miter bend in a pipe line causes separation of the fluid from the solid boundary at the inner juncture of the bend. The resulting contraction and subsequent expansion of the flow downstream from the bend produce a dissipation of energy which is primarily attributable to eddy diffusion. The head loss can thus be approximated by the conventional equation for an abrupt expansion. In dimensionless form this is

$$\frac{h_L}{V_0^2/2g} = \left(\frac{1}{C_c} - 1\right)^2 \tag{1}$$

in which h_L is the loss in head, $V_0^2/2g$ is the velocity head in the pipe with fully expanded flow, and C_c is the ratio of the contracted

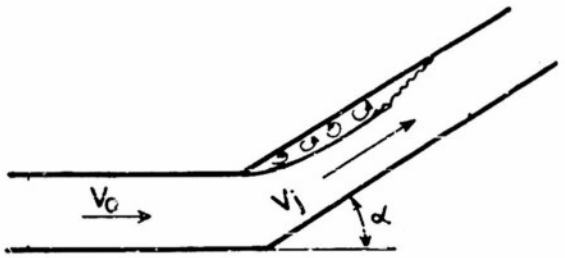

FIG. 1. FLOW PATTERN IN A MITER BEND.

area to the area of the pipe—a type of coefficient of contraction. A schematic representation of the flow is shown in Fig. 1.

Determination of the contraction coefficient, therefore, suffices for an estimate of the head loss. It is the purpose of this study to determine to what degree the contraction coefficient of the miter bend in a pipe can be approximated by an analysis of its two-dimensional counterpart

The two-dimensional miter bend (Fig. 2a) consists of three

*Now Assistant Professor, Department of Civil Engineering, University of Tennessee, Knoxville.

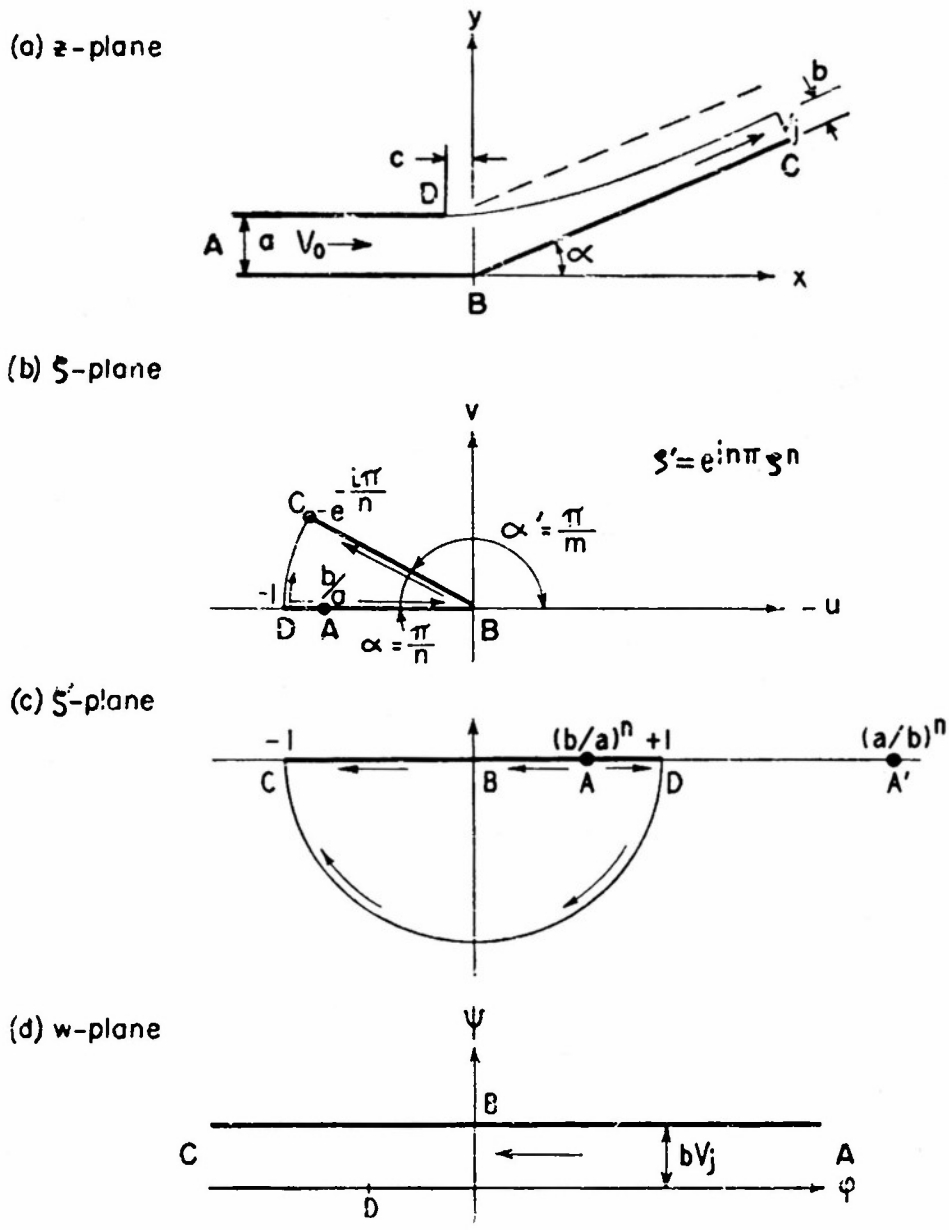

FIG. 2. TRANSFORMATION PLANES.

semi-infinite planes which serve as solid boundaries to the flow, the remainder of the boundary being a curved surface of separation upon which a constant pressure is presumed to act. The planes BA and BC form the outer boundary, intersecting with the deflection angle α at the point B (chosen as the origin for $z = x + iy$). The inner solid boundary DA is parallel to BA and separated from it by a distance a. The free surface DC is a curve and becomes

parallel to BC asymptotically, the ultimate thickness of the jet being b. The point of separation D is defined by the abscissa c and the ordinate a. The dashed line extending downstream from D represents the position of the downstream portion of the inner wall.

Since the pressure is assumed to be constant along the free surface, it follows that the velocity along the surface varies in direction only. Inasmuch as either the magnitude or the direction of the velocities along all boundaries is constant, the necessary requirements for application of the free-streamline theory are fulfilled.

The problem can be considered as the determination of the coefficient of contraction $C_c = b/a$ in terms of the angle α and the coordinates of the point of separation D—that is, the definition of the function f in the equation

$$\frac{b}{a} = f\left(\alpha, \frac{c}{a}\right) \tag{2}$$

Mathematically, however, it is more convenient to solve for c for given values of the deflection angle and contraction coefficient.

The solution parallels that of the paper by Messrs. Siao and Hubbard since the present problem is, in effect, an extension of the problem treated therein. The flow pattern is first transformed to the ordinary hodograph by the basic relationship

$$\zeta = \frac{1}{V_j}\frac{dw}{dz} = -\frac{u}{V_j} + i\frac{v}{V_j} = -\frac{q}{V_j}e^{-i\theta}$$

Since the velocity along the free streamline has the constant magnitude V_j, DC appears as a circular arc in the ζ-plane. The solid boundaries become radial lines with their terminal points located as shown in Fig. 2b.

If the angle α is set equal to π/n, n being an integer greater than unity, the flow pattern can be simplified further by the auxiliary transformation

$$\zeta' = (-\zeta)^n = e^{i\pi n}\zeta^n \tag{3}$$

In the ζ'-plane, the entire solid boundary falls on the real axis (Fig. 2c).

By means of the method of images, the given flow pattern in the ζ'-plane is obtained directly from the locating of point sources of strength $2aV_j$ at A and A' ($\zeta'_{A'} = [a/b]^n$) and a sink of double

strength at B. Although the complete pattern is symmetrical about the real axis, only the lower half of the ζ'-plane is relevant. The complex potential is then written immediately:

$$w = \phi + i\psi = \frac{2bV_j}{\pi} \ln (\zeta' + 1) - \frac{bV_j}{\pi} \ln [\zeta' - (b/a)^n]$$

$$- \frac{bV_j}{\pi} \ln [\zeta' - (a/b)^n] = \frac{bV_j}{\pi} \Big\{ 2 \ln (e^{i\pi n} \zeta^n + 1)$$

$$- \ln [e^{i\pi n} \zeta^n - (b/a)^n] - \ln [e^{i\pi n} \zeta^n - (a/b)^n] \Big\} \qquad (4)$$

The complex coordinate of point D in the z-plane is

$$c + ia = \oint_{CD} dz = \oint_{CD} \frac{1}{V_j} \frac{dw}{\zeta} = \int_0^1 \frac{b}{\zeta \pi} \Big[\frac{2}{e^{i\pi n} \zeta^n + 1} - \frac{1}{e^{i\pi n} \zeta^n - (b/a)^n}$$

$$- \frac{1}{e^{i\pi n} \zeta^n - (a/b)^n} \Big] n e^{i\pi n} \zeta^{n-1} d\zeta = \frac{nb}{\pi} \int_0^1 \Big[\frac{2}{\zeta^n + e^{-i\pi n}}$$

$$- \frac{1}{\zeta^n - e^{-i\pi n}(b/a)^n} - \frac{1}{\zeta^n - e^{-i\pi n}(a/b)^n} \Big] \zeta^{n-2} d\zeta \qquad (5)$$

Equation (5) consists of the sum of three integrals of the type

$$\int_0^1 \frac{\zeta^{n-2} d\zeta}{\zeta^n - K^n}$$

in which K is a complex constant. Since n is a positive integer the integration can be completed by substituting for each of these terms a polynomial expansion of n terms,

$$\frac{\zeta^{n-2} d\zeta}{\zeta^n - K^n} = \frac{1}{nK} \sum_{r=0}^{n-1} \frac{e^{-i2r\pi/n}}{(\zeta/K) - e^{i2r\pi/n}} d(\zeta/K)$$

whence

$$\int_0^1 \frac{\zeta^{n-2} d\zeta}{\zeta^n - K^n} = \frac{1}{nK} \sum_{r=0}^{n-1} e^{-i2r\pi/n} \ln \left(1 - \frac{e^{-i2r\pi/n}}{K}\right)$$

If the above relationship is substituted into Eq. (5), simplified, and separated into real and imaginary terms, the value of c/b is obtained:

$$\frac{c}{b}=\frac{1}{\pi}\sum_{r=0}^{n-1}\left\{-\cos\left(\frac{2r+1}{n}\pi\right)\ln\left[2-2\cos\left(\frac{2r+1}{n}\pi\right)\right]\right.$$
$$\left.+\left(\frac{2r+1-n}{n}\pi\right)\sin\left(\frac{2r+1}{n}\pi\right)\right\}+\frac{1}{\pi}\sum_{r=0}^{n-1}\frac{a}{b}\left\{\frac{1}{2}\cos\left(\frac{2r}{n}\pi\right)\ln\left[1\right.\right.$$
$$\left.-2\frac{a}{b}\cos\left(\frac{2r}{n}\pi\right)+\left(\frac{a}{b}\right)^2\right]+\sin\left(\frac{2r}{n}\pi\right)\tan^{-1}\left[\frac{\sin(2r\pi/n)}{(b/a)-\cos(2r\pi/n)}\right]\Bigg\}$$
$$+\frac{1}{\pi}\sum_{r=0}^{n-1}\frac{b}{a}\left\{\frac{1}{2}\cos\left(\frac{2r}{n}\pi\right)\ln\left[1-2\frac{b}{a}\cos\left(\frac{2r}{n}\pi\right)+\left(\frac{b}{a}\right)^2\right]\right.$$
$$\left.+\sin\left(\frac{2r}{n}\pi\right)\tan^{-1}\left[\frac{\sin(2r\pi/n)}{(a/b)-\cos(2r\pi/n)}\right]\right\} \tag{6}$$

For $\alpha \geqq \pi/2$ the supplementary angle α' is defined by

$$\alpha' = \pi - \frac{\pi}{n} = \frac{\pi}{m}$$

from which

$$n = \frac{m}{m-1}$$

If the indicated substitution is made in Eq. (6), the value of c/b corresponding to an angle greater than $\pi/2$ is obtained through steps differing only in detail from the integration procedure outlined above:

$$\frac{c}{b}=\frac{1}{\pi}\sum_{r=0}^{m-1}\left\{-\cos\left(\frac{2r+1-m}{m}\pi\right)\ln\left[2-2\cos\left(\frac{2r+1}{m}\pi\right)\right]\right.$$
$$\left.+\left(\frac{2r+1-m}{m}\pi\right)\sin\left(\frac{2r+1-m}{m}\pi\right)\right\}+\frac{1}{\pi}\sum_{r=0}^{m-1}\frac{a}{b}\left\{\frac{1}{2}\cos\left(\frac{2r}{m}\pi\right)\ln\left[1\right.\right.$$
$$\left.-2\left(\frac{a}{b}\right)^{\frac{1}{m-1}}\cos\left(\frac{2r}{m}\pi\right)+\left(\frac{a}{b}\right)^{\frac{2}{m-1}}\right]-\sin\left(\frac{2r}{m}\pi\right)F_1(m)\Bigg\}$$
$$+\frac{1}{\pi}\sum_{r=0}^{m-1}\frac{b}{a}\left\{\frac{1}{2}\cos\left(\frac{2r}{m}\pi\right)\ln\left[1-2\left(\frac{b}{a}\right)^{\frac{1}{m-1}}\cos\left(\frac{2r}{m}\pi\right)+\left(\frac{b}{a}\right)^{\frac{2}{m-1}}\right]\right.$$
$$\left.-\sin\left(\frac{2r}{m}\pi\right)F_2(m)\right\} \tag{7}$$

in which

$$F_1(m)=\tan^{-1}\frac{\sin\left(\frac{2r}{m}\pi\right)}{\left(\frac{b}{a}\right)^{\frac{1}{m-1}}-\cos\left(\frac{2r}{m}\pi\right)} \quad , \quad F_2(m)=\tan^{-1}\frac{\sin\left(\frac{2r}{m}\pi\right)}{\left(\frac{a}{b}\right)^{\frac{1}{m-1}}-\cos\left(\frac{2r}{m}\pi\right)}$$

From Eqs. (6) and (7) the desired quantity c/a for the various specific values of α corresponding to $n = 2, 3, 4$ and $m = 3, 4$

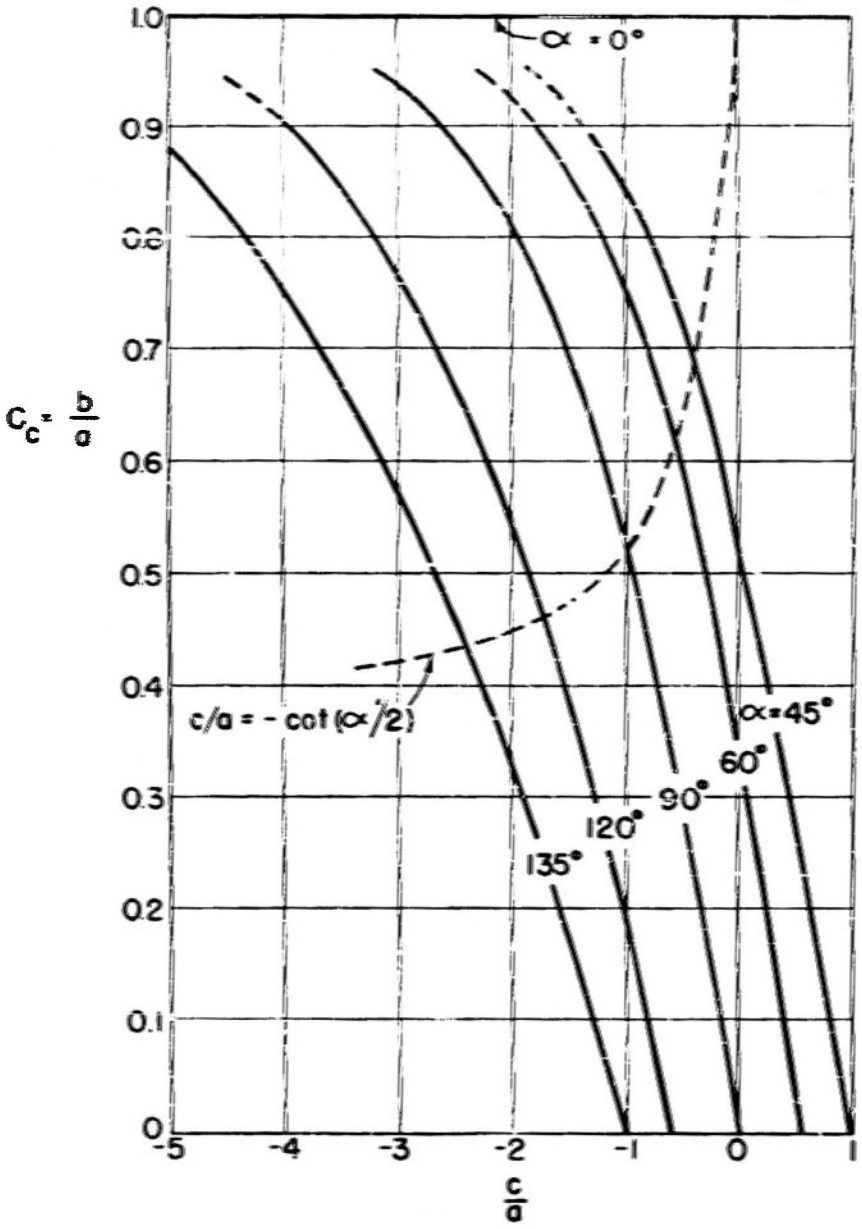

FIG. 3. CONTRACTION COEFFICIENTS.

can be obtained as functions of b/a. The results are plotted in Fig. 3, which is the graphical representation of Eq. (2). In particular, the functional relationship between c/a and b/a for $\alpha = \pi/2$ can be shown to be identical with that obtained by McNown and Hsu [12] for the special case of total lateral efflux from a two-dimensional conduit with a semi-infinite barrier.

In Fig. 3, for each value of α, b/a must equal zero for $c/a = \cot \alpha$. The limit of unity is approached by b/a for all angles between 0 and π as c/a becomes very large negatively. With $\alpha = 0$, b/a is equal to unity for all real values of c/a, whereas for α approaching π, b/a approaches zero for all real values of c/a.

Superposed on Fig. 3 is the locus of b/a for the especially interesting case in which point D lies on the bisector of the supplementary angle α'; that is, for $c/a = -\cot \alpha'/2$. This case defines

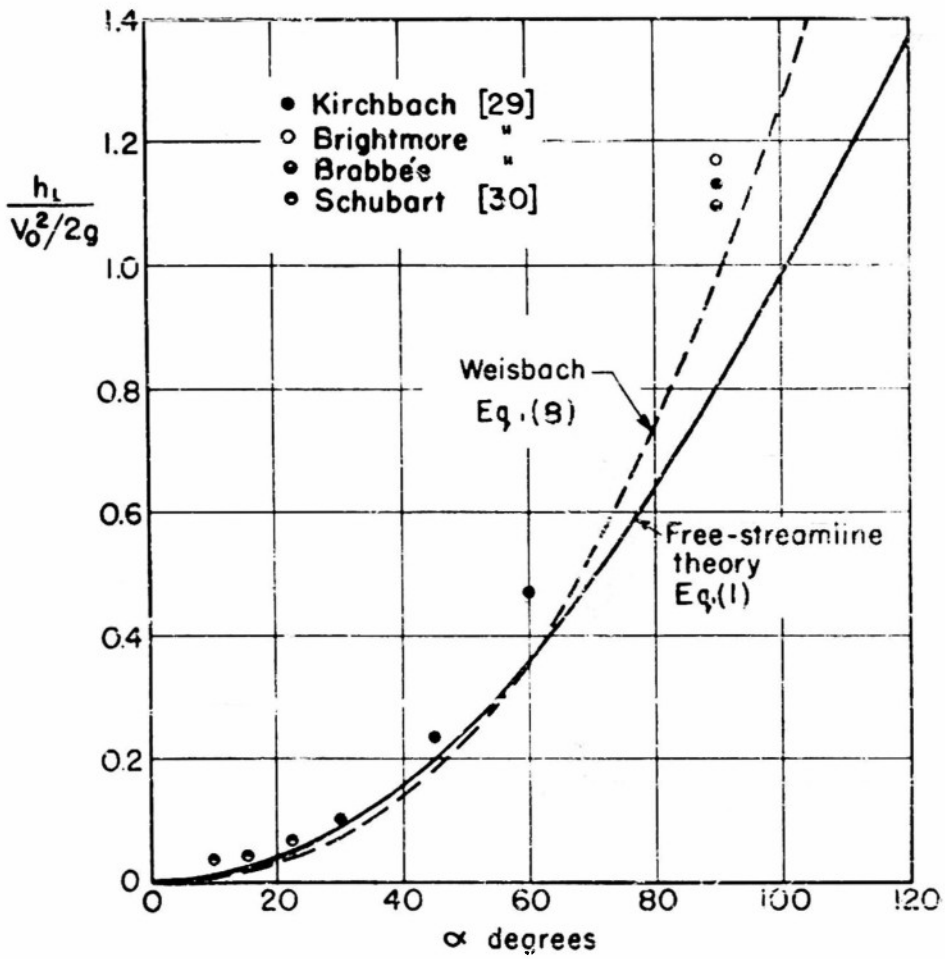

FIG. 4. HEAD LOSS IN MITER BENDS OF VARIOUS ANGLES.

the equivalent contraction coefficient for the usual design of miter bends.

Finally, Fig. 4 shows a plot of head loss in miter bends for various angles based on the substitution of b/a from Fig. 3 for C_c in Eq. (1). Included in the figure are typical experimental results [29, 30, 31]. Values for the Weisbach curve [32] were calculated from the empirically determined equation

$$\frac{h_L}{V_0^2/2g} = 0.9457 \sin^2 \frac{\alpha}{2} + 2.047 \sin^4 \frac{\alpha}{2} \tag{8}$$

The agreement of experimental data with the curve calculated by Eq. (1) and the free-streamline theory is good for small to moderate deflection angles but shows increasingly poorer correlation for larger angles. This, however, is to be expected in view of the increasing importance of the secondary flow pattern and the resulting secondary losses with increasing bend angle.

REFERENCES

1. Helmholtz, H., "Über discontinuirliche Flüssigkeitsbewegungen," *Monatsberichte Akad d. Wiss. Berlin*, 1868. pp. 215-228.
2. Kirchhoff, G., "Zur Theorie freier Flüssigkeitsstrahlen," Crelle, Vol. 70, 1869, pp. 289-298.
3. Lord Rayleigh, "Notes on Hydrodynamics," *Phil. Mag.*, Dec. 1876
4. Mises, R. v., "Berechnung von Ausfluss und Ueberfallzahlen," *VDI Zeitschrift*, 1917, pp. 447-462.
5. Birkhoff, G., Plesset, M., and Simmons, N., "Wall Effects in Cavity Flow," *Q. Appl. Mech.*, Vol. 8, 1950, pp. 151-168 and Vol. 9, 1952, pp. 413-421.
6. Plesset, M. S., and Shaffer, P. A. Jr., "Cavity Drag in Three Dimensions," *J. of Appl. Phys.*, Vol 19, 1948, pp. 934-939.
7. Michell, J. H., "On the Theory of Free Streamlines," *Phil. Trans. Roy. Soc. London*, Ser. A, Vol. 181, 1890, pp. 389-431.
8. Planck, M., "Zur Theorie der Flüssigkeitsstrahlen," *Ann. Phys. u. Chem.*, Vol. 21, 1884, pp. 499-509.
9. Christoffel, E. B., "Sul Problema delle Temperature Stazionarie e la rappresentazione di una Data Superficie," *Ann. di Mat.*, 2da Ser., Vol. I, 1867, pp. 95-103.
10. Schwarz, H. A., "Notizia sulla rappresentazione conforme di un'area ellittica sopra un'area circolare," *Ann. di Mat.*, 2da Ser., Vol. III, 1869, p. 166.
11. Salzman, F., "Blade-Clearance Leakage Losses in Steam Turbines," *Escher-Wyss News*, Vol. 8, 1935, pp. 95-102.
12. McNown, J. S., and Hsu, E. Y., "Application of Conformal Mapping to Divided Flow," *Proc. of the Midwestern Conference on Fluid Dynamics*, J. W. Edwards, 1951, pp. 143-155.
13. Birkhoff, G., *Hydrodynamics*, Princeton, 1950.
14. Lamb, H., *Hydrodynamics*, Dover, 1945.
15. Rouse, H., and Abul-Fetouh, A. H., "Characteristics of Irrotational Flow through Axially Symmetric Orifices," *ASME Trans.*, Vol. 17, No. 4, Dec. 1950.
16. Rouse, H., and McNown, J. S., "Cavitation and Pressure Distribution," *S.U.I. Studies in Engineering*, Bull. 32, 1948.
17. Eisenberg, P., and Pond, H. L., "Water Tunnel Investigations of Steady State Cavities," *David Taylor Model Basin Report 668*, Oct. 1948.
18. Eisenberg, P., "On the Mechanism and Prevention of Cavitation," *David Taylor Model Basin Report 712*, July 1950, pp. 41-42.

19. Réthy, M., "Strahlenformen incompressibler reibungsloser Flüssigkeiten," *Mathematische Annalen*, Vol. 46, 1895, pp. 249-272.

20. Cisotti, U., *Idromeccanica Piana*, Vol. 2, Libreria Editrice Politecnica, Milano, 1922, pp. 293-299.

21. Elder, R. A., and Dougherty, G. B. "Characteristics of Fixed-Dispersion Cone Valves," *ASCE Proceedings Separate No. 153*, Sept. 1952.

22. Greenhill, G., "Theory of a Stream Line Past a Plane Barrier," *Reps. and Memos. No. 19*, Adv. Comm. Aero. (Great Britain), 1910, pp. 26-29.

23. Milne-Thomson, L. M., *Jacobian Elliptic Function Tables*, Dover, New York, 1950.

24. Neville, E. H., *Jacobian Elliptic Functions*, Clarendon, Oxford, 2nd Ed., 1951.

25. Love, A. E. H., "On the theory of Discontinuous Fluid Motion . . . ," *Proc. Cambridge Phil. Soc.*, Vol. 7, 1889-1892.

26. "Laboratory Tests on Models of Lock Hydraulic Structures;" *Hydraulic Laboratory Report No. 52*, U. S. Corps of Engineers, St. Paul Dist. Suboffice, Iowa City, Iowa, June 1946.

27. "Filling and Emptying Systems for New Cumberland Locks, Ohio River;" *Hydraulic Laboratory Report No. 56*, U. S. Corps of Engineers, St. Paul Dist. Suboffice, Iowa City, Iowa, August 1952.

28. McNown, J. S., "Mechanics of Manifold Flow," *ASCE Proceedings Separate No. 258*, Aug., 1953.

29. Kirchbach, H., "Loss of Energy in Miter Bends," *Trans. Munich Hydr. Inst.*, Bull. 3, English translation, ASME, 1935, pp. 43-64.

30. Schubart, W., "Energy Loss in Smooth- and Rough-Surfaced Bends and Curves in Pipe Lines," *loc. cit.*, pp. 81-100.

31. Kaufmann, W., *Hydromechanik*, Band II, Springer, 1934, p. 91.

32. Weisbach, J., *Lehrbuch der Ingenieur- und Machinenmechanik*, Band I, J. Vieweg, Braunschweig, 1875, p. 1043.

COLLEGE OF ENGINEERING
STATE UNIVERSITY OF IOWA

Complete undergraduate courses are offered in Chemical, Civil, Commercial, Electrical, and Mechanical Engineering, as well as graduate courses in these fields and in Mechanics and Hydraulics. For detailed information, application may be made to T. H. MeCarrel, Registrar, State University of Iowa, Iowa City, Iowa.

IOWA INSTITUTE OF HYDRAULIC RESEARCH

The Institute was organized to coordinate the talents and facilities available at the University of Iowa for the investigation of problems in the fields of fluid mechanics, hydrology, and hydraulic engineering. Through this medium the University has cooperated with government agencies, technical societies, and industrial concerns throughout the country and abroad. Correspondence regarding the services of the Institute should be addressed to Hunter Rouse, Director, Iowa Institute of Hydraulic Research, Iowa City, Iowa.

STUDIES IN ENGINEERING

Bulletin 1. "The Flow of Water Through Culverts," by D. L. Yarnell, F. A. Nagler, and S. M. Woodward, 1926. 128 pages, 26 figures, 23 plates. Out of print.

Bulletin 2. "Laboratory Tests on Hydraulic Models of the Hastings Dam," by Martin E. Nelson, 1932. 72 pages, 40 figures. Out of print.

Bulletin 3. "Tests of Anchorages for Reinforcing Bars," by Chesley J. Posey, 1933. 32 pages, 18 figures, price $0.50.

Bulletin 4. "The Physical and Anti-Knock Properties of Gasoline Blends," by Theodore R. Thoren, 1934. 32 pages, 13 figures, price $0.35.

Bulletin 5. "The Transportation of Detritus by Flowing Water—I," by F. T. Mavis, Chitty Ho, and Yun-Cheng Tu, 1935. 56 pages, 15 figures, price $0.50.

Bulletin 6. "An Investigation of Some Hand Motions Used in Factory Work," by Ralph M. Barnes, 1936. 60 pages, 22 figures. Out of print.

Bulletin 7. "A Study of the Permeability of Sand," by F. T. Mavis and Edward F. Wilsey, 1936. 32 pages, 12 figures, price $0.35.

Bulletin 8. "Radiation Intensities and Heat-Transfer in Boiler Furnaces," by Huber O. Croft and C. F. Schmarje, 1936. 32 pages, 17 figures, price $0.35.

Bulletin 9. "A Summary of Hydrologic Data, Ralston Creek Watershed, 1924-35," by F. T. Mavis and Edward Soucek, 1936. 72 pages, 25 figures, price $0.50.

Bulletin 10. "Report on Hydraulics and Pneumatics of Plumbing Drainage Systems—I," by F. M. Dawson and A. A. Kalinske, 1937. 32 pages, 5 figures, price $0.35.

Bulletin 11. "The Transportation of Detritus by Flowing Water—II," by F. T. Mavis, Te-Yun Liu, and Edward Soucek, 1937. 32 pages, 8 figures, price $0.35.

Bulletin 12. "Studies of Hand Motions and Rhythm Appearing in Factory Work," by Ralph M. Barnes and Marvin E. Mundel, 1938. 64 pages, 24 figures. Out of print.

Bulletin 13. "Hydraulic Tests of Small Diffusers," by F. T. Mavis, Andreas Luksch, and Hsi-Hou Chang, 1938. 32 pages, 16 figures, price $0.25.

Bulletin 14. "A Study in Flood Waves," by Elmer E. Moots, 1938. 32 pages, 7 figures, price $0.25.

Bulletin 15. "The Road Map of Hydraulic Engineering in Iowa," by E. W. Lane and Edward Soucek, 1938. 16 pages, 4 figures, price $0.25.

Bulletin 16. "A Study of Hand Motions Used in Small Assembly Work,"

by Ralph M. Barnes and Marvin E. Mundel, 1939. 68 pages, 33 figures, price $0.50.

Bulletin 17. "A Study of Simultaneous Symmetrical Hand Motions," by Ralph M. Barnes and Marvin E. Mundel, 1939. 40 pages, 15 figures, price $0.40.

Bulletin 18. "Percolation and Capillary Movements of Water Through Sand Prisms," by F. T. Mavis and Tsung-Pei Tsui, 1939. 32 pages, 13 figures, price $0.25.

Bulletin 19. "Two Decades of Hydraulics at the University of Iowa, Abstracts of Theses, Publications, and Research Reports, 1919-1938," edited by F. T. Mavis, 1939. 84 pages, price $0.50.

Bulletin 20. "Proceedings of Hydraulics Conference," edited by J. W. Howe, 1941. 233 pages, 84 figures. Out of print.

Bulletin 21. "Studies of One and Two-Handed Work," by Ralph M. Barnes, Marvin E. Mundel, and John M. MacKenzie, 1940. 68 pages, 31 figures, price $0.50.

Bulletin 22. "The Study of the Effect of Practice on the Elements of a Factory Operation," by Ralph M. Barnes and James S. Perkins with the assistance and collaboration of J. M. Juran, 1940. 96 pages, 31 figures, price $0.75.

Bulletin 23. "An Annotated Bibliography of Fishways," by Paul Nemenyi, 1941. 72 pages, 12 figures, price $0.50.

Bulletin 24. "An Investigation of Fishways," by A. M. McLeod and Paul Nemenyi, 1941. 64 pages, 15 figures, 6 plates, price $0.50.

Bulletin 25. "The Electrostatic Effect and the Heat Transmission of a Tube," by Melvin R. Wahlert and Huber O. Croft, 1941. 40 pages, 10 figures, price $0.40.

Bulletin 26. "Investigations of the Iowa Institute of Hydraulic Research," 1939-1940, edited by J. W. Howe, 1941. 64 pages, 15 figures, price $0.40.

Bulletin 27. "Proceedings of the Second Hydraulics Conference," edited by J. W. Howe and Hunter Rouse, 1943. 352 pages, 167 figures, price $1.65.

Bulletin 28. "The Preparation of Stoker Coals from Iowa Screenings," by H. L. Olin, 1942. 64 pages, 22 figures, price $0.50.

Bulletin 29. "Study of Transportation of Fine Sediments by Flowing Water," by A. A. Kalinske and C. H. Hsia, 1945. 40 pages, 18 figures, price $0.40.

Bulletin 30. "The Iowa Institute of Hydraulic Research," 1946. 80 pages, 36 figures, price $0.50.

Bulletin 31. "Proceedings of the Third Hydraulics Conference," edited by J. W. Howe and John S. McNown, 1947. 332 pages, 163 figures, price $2.50.

Bulletin 32. "Cavitation and Pressure Distribution—Head Forms at

Zero Angle of Yaw," by Hunter Rouse and John S. McNown, 1948. 70 pages, 53 figures, price $1.00.

Bulletin 33. "Third Decade of Hydraulics at the State University of Iowa," edited by M. C. Boyer, 1949. 84 pages, 8 figures, price $0.50.

Bulletin 34. "Proceedings of the Fifth Hydraulics Conference," edited by John S. McNown and M. C. Boyer, 1953, 302 pages, 139 figures, price $3.50.

Bulletin 35. "Free-Streamline Analyses of Transition Flow and Jet Deflection," edited by John S. McNown and Chia-Shun Yih, 1953, 82 pages, 37 figures, price $1.00.